

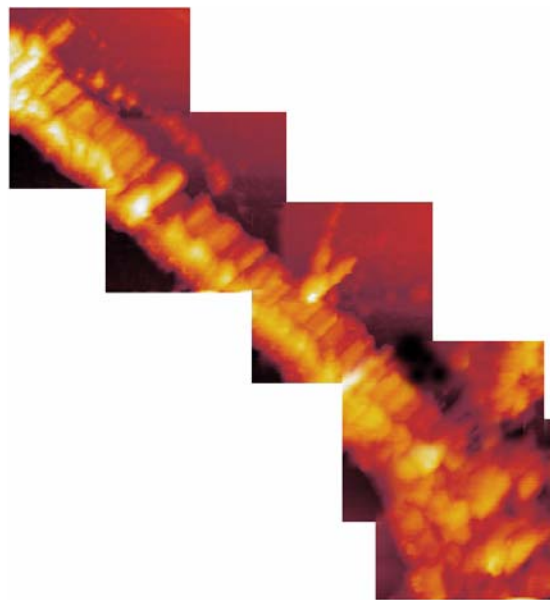


February 2007

Physics Master Project

**Rapport de travail pratique pour l'obtention du diplôme de
Physicien EPF**

High resolution imaging of neuronal receptors by Scanning Near-field Optical Microscopy



Bernard Lanz

Supervisor:

External Expert:

Assistant:

Prof. Davor Pavuna, LPRX, EPFL

Prof. Antonio Cricenti, ISM-CNR, Rome, Italy

Johanna Generosi, LPRX, EPFL

Abstract

This report presents a fluorescence imaging study on neuron cells performed by Scanning Near-field Optical Microscopy (SNOM). This recent experimental observation tool, still in development, aims for subwavelength optical resolution images, surpassing in that way the possibilities of the classical microscopy.

Our study is focused on rats' neurons which glutamate receptors are labeled with fluorophores. Glutamate receptors are the primary mediators of excitatory synaptic transmission in the mammalian central nervous system. The changes in their number underlie aspects of synaptic plasticity and information storage in the brain. The comprehension of their trafficking through the neuron body is thus essential to understand the different functionalities and illnesses of the brain.

Our SNOM setup is able to provide the topography, the fluorescence emission map and the optical transmission properties of the neuron samples. We present high resolution transmission images and determine their resolution with wavelet analysis. These images offer new information about the inner constituents of the cells. The fluorescence images are treated and interpreted in conjunction with the topography and the optical transmission. Without giving single receptor resolution, they show a non uniform surface distribution of the receptors on the cell membrane with a higher concentration near the nucleus, thus confirming the biological models. We stress the intrinsic new information given by the fluorescence measurements, mainly independent from topographical or transmission artifacts.

Table of contents

Abstract

1. Historical background and introduction to our SNOM study	1
2. Theoretical background	3
2.1. Scanning Near-field Optical Microscopy	3
2.1.1. Evanescent waves and near-field	3
2.1.2. Aperture and apertureless SNOM	4
2.1.3. Advantages of each method	5
2.1.4. Movements of the probe	6
2.2. Possibilities of the scanning near-field optical microscopy	7
2.2.1. Infrared SNOM	7
2.2.2. Fluorescence SNOM	8
2.2.3. Raman spectroscopy with SNOM	10
2.3. Neuronal cells	11
3. Experimental setup	16
4. Experimental results and discussion	24
4.1. First results and transmission contrast	24
4.2. Topography images and gradient analysis	27
4.3. Resolution analysis	30
4.3.1. Two dimensional Fourier analysis	32
4.3.2. Discrete wavelet analysis	35
4.4. Fluorescence emission	43
4.4.1. Fluorescence correction	43
4.4.2. Global results and discussion	47
5. Conclusions and perspectives	51
6. Acknowledgments	52
7. Bibliography	53

1. Historical background and introduction to our fluorescence-SNOM study

The Scanning Near-field Optical Microscopy (SNOM) is part of the family of Scanning Probe Microscopies (SPM) which appeared in 1982 with the invention of the Scanning Tunneling Microscopy (STM) (G. Binnig, H. Rohrer, 1982). To cure the principal inconvenient of the STM, namely the impossibility of studying insulating samples, another type of local probe microscopy was proposed: the atomic force microscopy (AFM) (G. Binnig & al., 1986). The technological progresses done with this two types of microscopy contributed to the development of the SNOM.

The principal motivation to use the scanning near-field microscopy is to become independent from the wide-field diffraction limit. This limit affects the classical optical microscopy and makes it impossible to observe details smaller than half of the wavelength of the light used for the observation.

The first SNOM working with visible light was developed around 1984 by D.W. Pohl, W. Denk and M. Lanz (D.W. Pohl & al., 1984). This setup used a monochromatic light of 488 nm of wavelength and was able to reach a lateral resolution of about 25 nm ($\lambda/20$), which is much better than the best resolution achievable with a wide-field microscope.

Actually, other attempts were done earlier in other wavelength ranges. E. Ash and G. Nicholls (E. Ash and G. Nicholls, 1972) reached a resolution of $\lambda/60$ with a 0.5 mm aperture on a glass substrate covered by aluminium patterns imaged using microwave light.

The first person to think about near-field optical microscopy was the Irish physicist E. Synge in 1928 (E. Synge, 1928), which had the idea of making a very small aperture in a metallic screen and to move this screen point by point above the sample. The hole had to be smaller than the wavelength of the light used for observation. In that way, the

observation could become independent from all the diffraction limits, since the microscope didn't use lenses. Images were recorded point by point using a sensitive photodetector that collects the transmitted light through the sample. So, the signal recorded at each point would be just one pixel of the final image. The new resolution limits were then the dimension of the probe and the distance between the probe and the sample. His experimental setup would have been actually very similar to those used nowadays, but Syngé never turned his ideas into reality. Nowadays, the hole has been replaced in most of the case by a tip, which can be either a pulled and treated optical fiber or different types of scattering objects brought very near the sample surface, typically nearer than 10nm.

SNOM is among others a useful tool to analyze biological samples. The molecular biologists need more and more fine observations on cells to understand how their metabolism is working. The objects under interest become smaller and smaller. Nowadays, the observations are oriented on macromolecules, mostly proteins, which have very specific functions like chemical receptors or ion channels. The optical measurements give potentially most information about these molecules. The high resolution of the SNOM is for this purpose expedient. Most of the studies are oriented towards fluorescence observations on specific labeled macromolecules. Some results on Ca^{2+} ion channels of cardiac cells (A. Ianoul & al., 2004) and on cell surface receptors of dendritic cells (M. Koopman & al., 2004) are examples of the possibilities of the SNOM in this field. A clear subwavelength resolution is reached.

We present in this report a fluorescence-SNOM study on rat's hippocampal neurons which alpha-amino-3-hydroxy-5-methyl-4-isoxazolepropionic acid (AMPA) receptors are labeled with Alexa 488. The position of these receptors in the neurons helps to understand the mechanism of their traffic and thus of their role in the change of the neurons' connections. We record also the transmitted light passing through the biological material. The transmitted light, without being as specific as the fluorescence, opens a new dimension in SNOM observations since it can also give subwavelength information about the optical density of the sample. We record in that way for each observed area three

images: topography, fluorescence and transmission. We discuss in this report the information given by these three different measurements.

2. Theoretical background

2.1. Scanning near-field optical microscopy:

2.1.1. Evanescent waves and near-field:

The motivation of developing SNOM instruments is that common wide-field microscopes reach in the best conditions a resolution of half the wavelength of the light source used (about 300 nm). This is known as the Rayleigh diffraction limit:

$$D = 0.61 \frac{\lambda}{n \sin \theta}$$

In this equation, D is the shortest distance between two points on a specimen that can still be distinguished as separate entities, λ is the wavelength of the light producing the image, n the refractive index of the medium separating the specimen and the objective lens, and θ the aperture half-angle of the optical system. (E. Abbe, 1873, B. Hecht & al., 2000)

Nowadays, there are a lot of types of SNOM, using different probes, working in transmission or in reflection, with far-field or evanescent lighting.

All the types of SNOM have the same theoretical basis: consider an object in a plane $(x,y,0)$. Consider a plane wave \vec{E} incident on a transverse plane $(x,y,0)$ propagating in the positive z direction. It can be shown that the reaction of the sample contains two types of components. For low spatial frequencies, the waves propagate in the z direction towards the observation plane. These components are the far-field components. The high spatial frequency components are only present near the sample and decay exponentially in the z direction. The region near the sample that contains the high spatial frequency components is called the near-field zone. (D. Courjon & C. Bainier, 2001)

So, the light containing the high spatial frequency information of the object does not propagate, but decays exponentially away from the object. SNOM allows the detection of these non-propagating evanescent waves in the near-field zone, thus giving the high spatial frequency information about the object. To detect the evanescent light, a probe is brought into the near-field zone, close to the sample. The dimension of the probe has to satisfy the condition of being smaller than $\lambda/2$, where λ is the wavelength used for imaging. A good description of the nature of the near-field is explained in the literature (A. Cricenti, 2005).

2.1.2. Aperture and apertureless SNOM:

To collect the sub-wavelength information of an object surface, several configurations are possible: either lighting the surface using evanescent waves which, diffracted by this surface, will produce homogeneous propagating waves containing the near-field information and detectable by a classical method, or lighting the surface by homogeneous waves which, diffracted by this surface, will produce evanescent waves carrying the near-field information collected by a nano-probe.

In the two methods, it is necessary to find a way to convert homogeneous waves in evanescent waves and vice versa. For E.Synge (E. Synge, 1928), the solution was a nano-hole. It can also be used as a nano-collector converting evanescent waves in homogeneous ones propagating in air or in a guide up to the detector. This hole should practically have very small dimensions.

A possibility consists in using the sharp end of a small object, considered as a nano-sized particle diffusing locally the near-field and able to play the role of converter. This is the principle of the apertureless SNOM. We can also notice that the penetration depth of evanescent waves is typically shorter than 100 nm. It will be necessary to bring the probe as near as possible to the surface. The resolution will be even better than the distance between sample and probe will be short. Actually, the more the probe is near the sample,

the more the SNOM acquires spatial high frequency information. In some configurations, it is possible to go down to some nanometers. (D. Courjon, C. Bainier, 2001)

On the other hand, the concept of the aperture probe is based on the same idea of nano-hole suggested by E. Synge. The role of this aperture is to confine the light in a very localized place of the sample. The probe is principally a waveguide with a tapered tip at the end with a very small sub-wavelength aperture, playing this role of nano-illuminator or nano-collector. This aperture can be used to light locally the sample (illumination mode); we detect in this case the propagating wave coming from this local interaction. The detection is done in the far-field, in reflection or more generally in transmission with the help of an optical system, like a microscope lens. The tip can also be used to detect locally the evanescent waves generated at the surface of the sample lighted in the far-field (detection mode). The field collected by the aperture becomes partially propagating by this interaction in the near-field and is guide to the other end of the fiber where it is detected by a photomultiplier and analyzed. We call it an aperture SNOM. The tip can be coated by a metal layer to improve its properties.

The aperture probe SNOM was the first to be used and is still the most widely used. It has a resolution down to 50 nm. The limited resolution of the aperture-based SNOM is due to the fact that reducing the aperture diameter, the number of photons that can pass through the aperture decreases. This in turn lowers the signal levels at the detector and decreases the signal-to-noise ratio, which imposes a conflicting limit on the resolution improvement that can be achieved by further reduction of aperture diameter.

2.1.3. Advantages of each method:

The apertureless SNOM has the disadvantage that the sample has to be illuminated from the far field. This can be a problem for light-sensitive samples, like those labeled with fluorophores which are affected by photobleaching. On the contrary, the aperture SNOM makes it possible to illuminate a localized zone. The noise of the near area is in this way also reduced. The main problem with aperture tips is to produce probes with reproducible

characteristics. Indeed, the techniques used to thin the optical probes don't permit the perfect reproducibility of the form and diameter before metallization (G.A. Valaskovic & al., 1995).

On the other hand, the present-day technology can produce atomically sharp apertureless tips. It means that apertureless SNOM can in principle achieve atomic optical resolution.

Another problem with the aperture SNOM is the lost of light in the thin end part of the fiber. This loss is a limit to the power of the incident wave on the sample, sometimes insufficient in spectroscopy-like experiments. A too powerful wave can in the worst case modify the form of the probe by heating or it can even melt the metallic coating (Haw-Long Lee & al., 2007).

On the other side, aperture SNOM makes it possible to analyze biological, dielectric, conductive or semi-conductive matter. We will focus our interest on fluorescently labeled biological samples, for which the aperture SNOM in illumination mode is appropriate.

2.1.4. Movements of the probe:

The two principle elements in a SNOM are the probe and the approach system controlling the distance between sample and tip. Both for aperture and apertureless SNOM, the tip has to be kept very near the sample to fulfill the near-field condition. In order to create an image of the sample, the probe is scanned over it, moving step by step and recording each time the optical properties of the area under the tip. In that way, it is possible to reconstruct an image in which each pixel is a measured quantity.

Since the near-field intensity depends strongly on the distance from the diffracting object, the probe has to be positioned at an equal distance of the sample surface in each point, even if there are high structures. To achieve this, the SNOM uses the short range interaction between the probe and the sample. The probe is fixed on an oscillating piezo-actuator (dither-piezo). When the tip comes near the surface, this interaction, called shear

force, damps the oscillation. A recording of the amplitude of oscillation gives information about how far the tip is from the sample. The idea is to change the z-position of the tip in order to keep a constant amplitude and thus to have a similar tip-sample distance in each point (B. Hecht & al., 2000).

The nature of the shear force is not really clear and is still a matter of debate. Van der Waals and capillary forces were first proposed. Some direct measurements of the shear forces were made and underlined the importance of a thin water layer present at the surface of the samples. The shear force can actually be decomposed in two parts: a constant component and a dither force which arises from an intermittent contact with the sample (D.A. Lapshin & al., 2002). This study also shows the importance of a usually neglected long range static attraction force which is dominant at small oscillation amplitudes.

2.2. Possibilities of the scanning near-field optical microscopy:

The SNOM is a spectroscopic technique by itself: it excites the sample in the near-field, making possible an independent analysis of very small areas and in the best case to do what is called single molecule spectroscopy. This is one of the most important features that make such a complicated setup useful. Spectroscopy is actually a general term to name all techniques that give information about the energy levels of the studied system, or about its dynamic. The technique used depends mostly on the energy source used to excite the sample. All types of spectroscopy have become very powerful because of the use of lasers as energy source. With some lasers, it is possible to define a frequency with a precision of twelve significant numbers! (D. Courjon and C. Bainier, 2001)

2.2.1. Infrared SNOM:

One way to analyze specific properties of a sample is the use of Infrared Scanning Near-field Optical Microscopy (IR-SNOM). This is actually a combination of infrared spectroscopy and scanning probe microscopy. The IR light is a quite low energy

electromagnetic radiation. In that way, it interacts with the vibration levels of the molecules. An energy step between two vibrational states of a chemical bond has a value which is typical of the chemical nature of the atoms attached by this bond and of the order of the bond. In this way, using the right IR wavelength for the source, it is possible to make a chemical selective absorption in the sample. The combination with an aperture SNOM enables to reach a fine lateral resolution. This opens a totally new research area since far-field observations limit the resolution to about $\lambda/2$ ($\sim 0.5\text{-}5\ \mu\text{m}$), which is huge if the interest is focused on local properties like for example in solid state physics or in biophysics, where the objects under interest are on a nanometer scale. Moreover, contrary to electron spectroscopy, IR spectroscopy has a deep penetration and can probe buried objects, which are frequently encountered in material sciences.

The IR-SNOM becomes a very useful tool if the IR source can be tunable. This property makes it possible to choose the molecule to observe and to obtain several maps of the same area, observing subsequently different chemical groups. An inconvenient of the SNOM is that the tip has a very low value of the transmittivity of the typical order of 10^{-5} (G.A. Valaskovic & al., 1995). Such a value demands a highly intense tunable light source. This condition is fulfilled by a free electron laser (FEL). Many interesting results on different types of sample have been realized with the FEL-SNOM combination. (A. Cricenti & al., 2004a), (A. Cricenti & al., 2004b)

2.2.2. Fluorescence SNOM:

Fluorescence SNOM is used to detect fluorescent molecules, which absorb efficiently one part of the visible spectrum or near UV and reemit after absorption a radiation shifted towards the large wavelengths. Most of these molecules are well-known fluorophores like the Alexa family. Alexa Fluor dyes are synthesized through sulfonation of coumarin, rhodamine, xanthene (such as fluorescein), and cyanine dyes. Sulfonation makes Alexa Fluor dyes negatively charged and hydrophilic. Alexa Fluor dyes are generally more stable, brighter, and less pH-sensitive than other standard dyes of comparable excitation and emission. The range of the excitation wavelengths of the different Alexa dyes goes

from 346nm to 749nm (N. Panchuk–Voloshina & al., 1999). It is also possible to use quantum dots or other fluorescent molecules like the Green fluorescent protein (GFP).

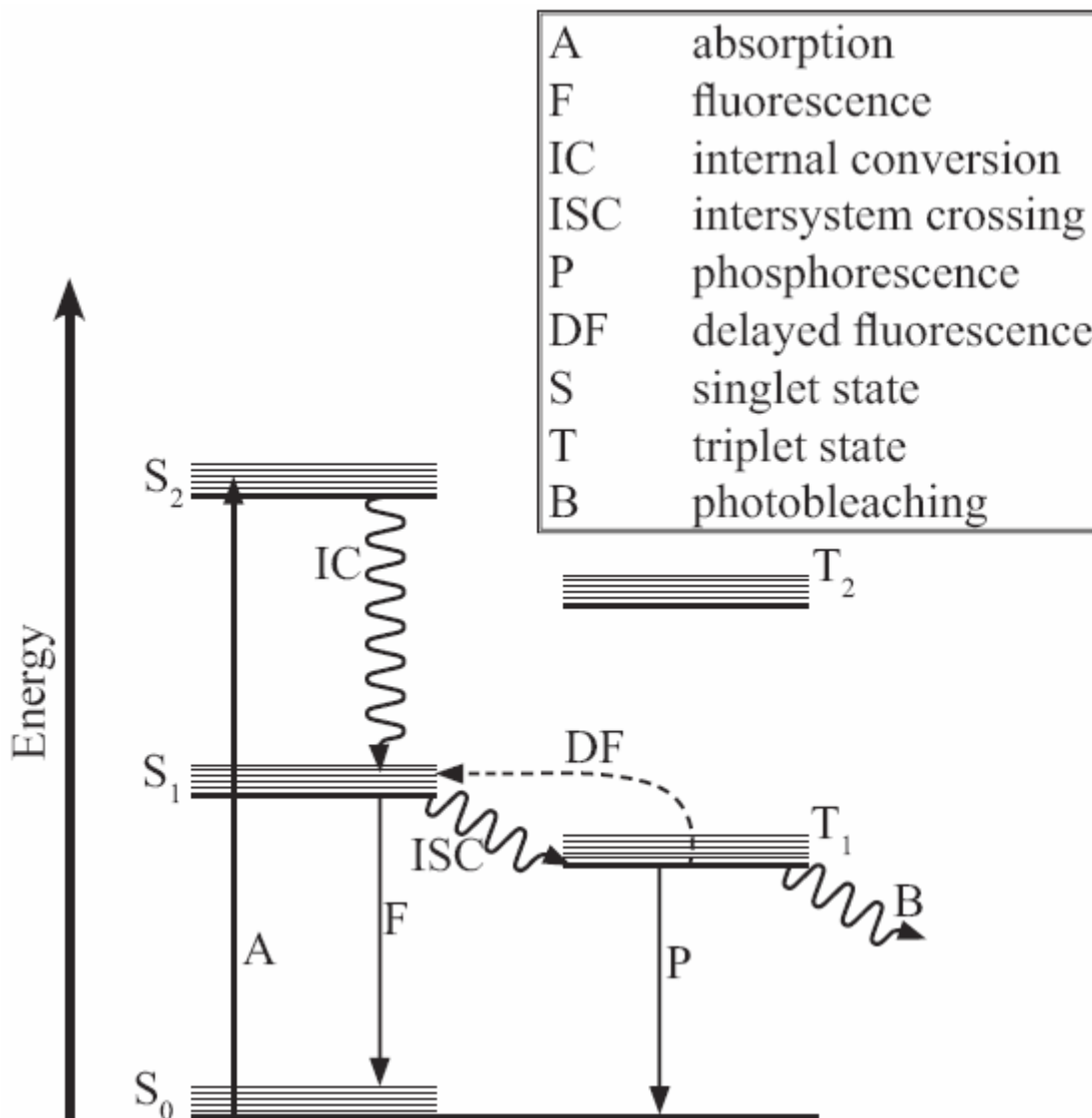


Fig. 1: Schematic representation of the principle of fluorescence called Jablonski Diagram.. The horizontal levels are the energy levels of the molecule, both electronic (thick lines) and vibrational (thin lines). The “parasit” cycle corresponds to the trapping in the triplet state (ISC) and the relaxation to S_0 called phosphorescence. Radiative transitions are indicated by straight arrows and nonradiative transitions by squiggly arrows.

If an incident photon has the right energy for the considered fluorescent molecule, the absorption effect annihilates the photon and brings the molecule in an excited electronic state. There are selection rules in the molecular physics which explains in details when

such a transition is possible (A. Callegari, 2005). The molecule is then in an excited vibrational state and relaxes slowly to the ground state in this new electronic potential. The fluorescence process consists in the return of the molecule in the electronic ground state by emission of another photon. This is again followed by a vibrational relaxation. The emitted photon has a lower energy than the one used for excitation. This is due to the two vibrational relaxations which are thermal dissipations. The reemitted light has therefore a longer wavelength. This phenomenon, known as the Stokes shift, is very useful to separate the incident light from the fluorescent emission by using filters. The Jablonski Diagram (figure 1) shows this principle.

The fluorophores are not working eternally. After a given time, they are subject to photobleaching. This is a photodynamic chemical reaction of excited fluorophores. It is mostly the reaction with highly reactive oxygen and it happens generally when the molecule is in the triplet state. After this reaction, the fluorescence cycle of the fluorophores is broken.

2.2.3. Raman spectroscopy with SNOM:

A molecule can interact with electromagnetic radiation in several ways. The fluorescence is an electronic excitation. The IR spectroscopy is due to the resonant absorption of light used by the molecule to change its vibrational state. The molecule can also diffuse the incident light. This diffusion can be either elastic or inelastic. In the inelastic case, the molecule can either take energy from the light to go in a vibrational excited state or give energy to the light by vibrational relaxation. This is called the Raman effect. In that way, light is coming simultaneously from the sample with the same wavelength as the incident beam (elastic scattering), with shorter wavelength (anti-Stokes Raman effect) and with larger wavelength (Stokes Raman effect) (G. Turrell & J. Corset, 1996). The change in the wavelength depends directly on the energy gaps between the vibrational levels. Each molecule or chemical group has then its own Raman spectrum. The recording of the total spectrum of the light passing through the sample gives in that way direct information about the identity of the different chemical constituents.

There are a lot of motivating objectives that nanometric Raman spectroscopy could reach. In fact, the spectrum of a molecule is affected by its environment. In that way, a measure of the pressure, the PH or different ions' concentration could be done. Far-field Raman spectroscopy gives a spectrum of a big population of molecules and all these values are averaged. On the contrary, the SNOM could give a high resolution map of these different local properties. For example, a good result about stress in a damaged silicon wafer has been done with near-field illumination (S. Webster & al., 1998).

2.3. Neuronal cells:

In this report, we present a study on neuronal cells. The samples are taken in the hippocampus of 7 days old rats. Their similitude with our human neurons makes it possible to collect important information about the neuronal system which might be useful to understand the functions and the illnesses of the brain.

The human brain consists of a vast network of more than 10^{11} nerve cells that communicate with each other through more than 10^{15} specialized cell junctions called synapses. The pattern of synaptic connections supports all aspects of brain function, from sensory perception and movement to learning and memory. The complexity of brain architecture is intimately associated with the inherent heterogeneous nature of neurons, since they can be classified into perhaps as many as 10000 different types. Differences in their structure, but also in their molecular content allow the generation of very different patterns of activity responsible for brain function. Understanding the development of neuron-neuron synapses is crucial to understand development of the nervous system abnormalities which underlie neurological and behavioral disorders.

The general structure of a neuron is shown in the figure 2. The electrochemical information called action potential always flow from the dendrites trough the cell body in the direction of the axon towards the synapses which are connected to dendrites and cell bodies of other neurons.

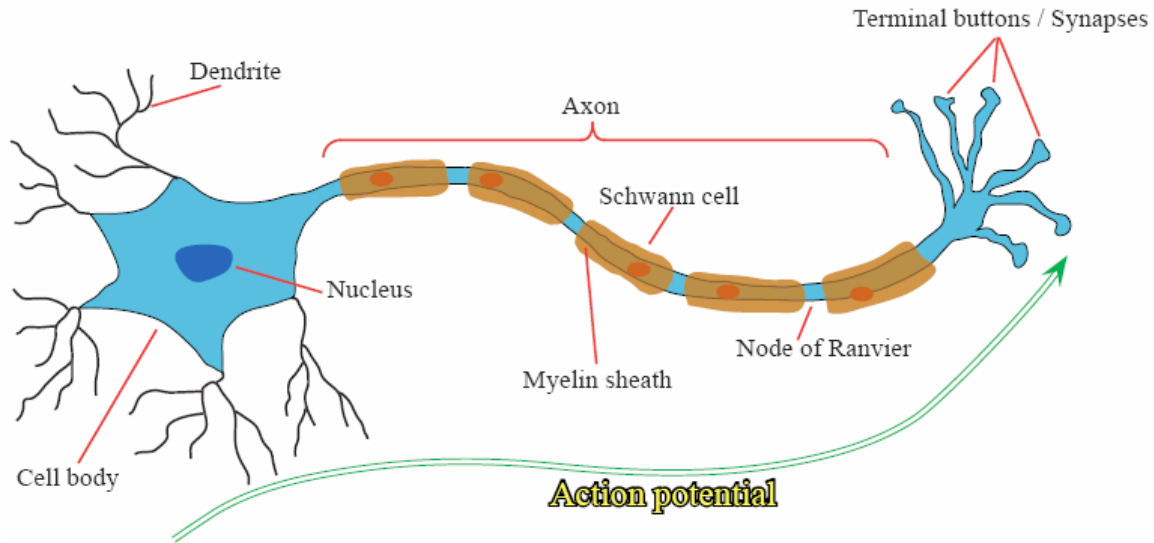
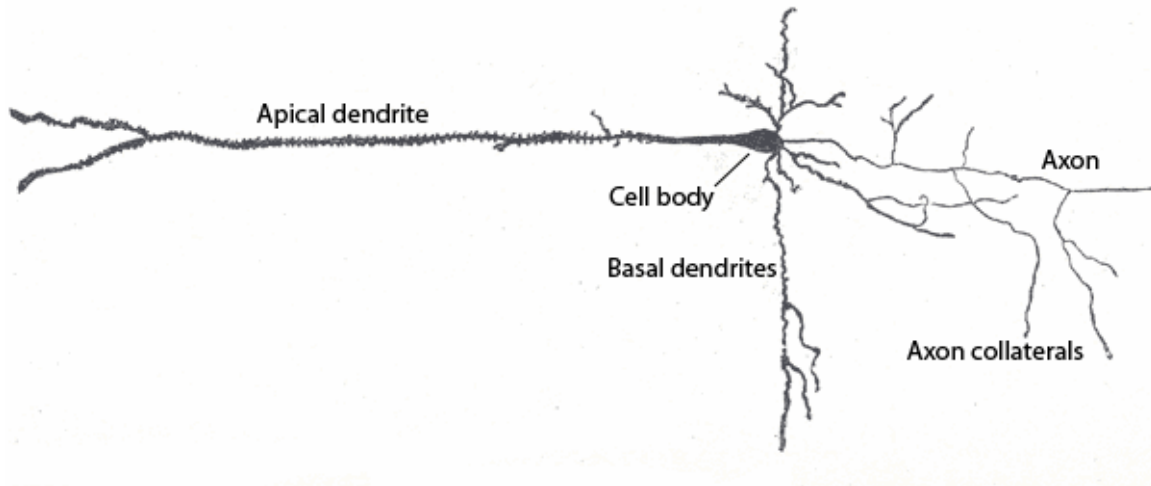


Fig. 2: Standard schematic view of a neuron

Axons and dendrites in the central nervous system are typically only about one micrometer thick, while some in the peripheral nervous system are much thicker. The cell body is usually about 10–25 micrometers in diameter and is often not much larger than the cell nucleus it contains. The axon, which carries the outgoing signal, can be very long. To accelerate the transmission of the signal, many neurons have insulating sheaths of myelin around the axon. This sheath is formed by glial cells and is regularly interrupted. These unsheathed regions are called Nodes of Ranvier and contain a high density of voltage-gated ion channels.

In this report, we show results taken on pyramidal neurons of the hippocampus of rats. These neurons have a slightly different structure shown in figure 3. They are multipolar neurons and have a triangularly shaped cell body and a thick dendrite with many small knobby dendritic spines. The base gives rise to a network of basal dendrites and an axon which has collaterals that synapse with other neurons in the cortex or in deeper regions of the brain (encyclopedia.thefreedictionary.com/Pyramidal+cells).



*Fig. 3: View of a typical pyramidal neuron of the hippocampus
(encyclopedia.thefreedictionary.com/Pyramidal+cells).*

Synapses are specialized intercellular junctions between neurons or between neurons and other excitable cells where signals are propagated from one cell to another. Synapses are defined as electrical or chemical depending upon whether transmission occurs via direct propagation of the electrical stimulus in the presynaptic process or via chemical intermediate. Electrical synapses are gap junctions between neurons, which allow bidirectional propagation of the signal and play a role in synchronizing neuronal activity (M.V.L. Bennett, 2000). However, most synapses are chemical synapses, sites of discontinuity of the neuronal network where propagation of the signal is highly regulated. At chemical synapses, referred to as synapses, the presynaptic electrical signal is converted into a secretory response, leading to the release of chemical intermediates, the neurotransmitters, into the synaptic cleft. This chemical message is then reconverted postsynaptically into an electrical signal along dendrites. Thus chemical synapses are fundamentally asymmetric, although some retrograde, feedback signaling does occur (Y. Goda & G.W. Davis, 2003). The basic feature of a synapse is a close apposition of specialized regions of the plasma membranes of the 2 participating cells to form the synaptic interface. On the presynaptic side, a cluster of neurotransmitter-filled synaptic vesicles is associated with the presynaptic plasma membrane. On the postsynaptic

membrane an accumulation of neurotransmitter receptors is marked by a thickening of the membrane.

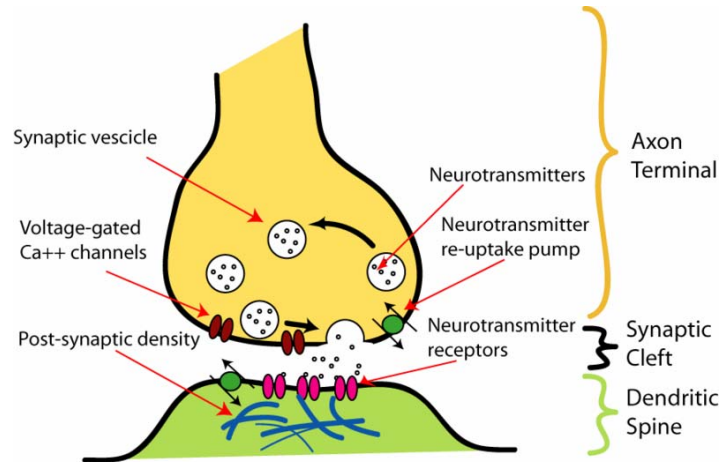


Fig. 4: Illustration of the major elements in a prototypical synapse. (en.wikipedia.org/wiki/Synapse)

In the mammalian brain, the majority of chemical synapses are excitatory and use glutamate as neurotransmitter. However, there is a great diversity of neurotransmitters which can lead to either an excitation or an inhibition of the postsynaptic cell. (P. Steiner, 2004)

Glutamate activates two types of postsynaptic receptors: ionotropic receptors (iGluRs), which are glutamate-gated cation channels, and metabotropic receptors (mGluRs), which are linked through G-proteins to second messengers systems. Ionotropic GluRs can be subdivided into three families on the basis of pharmacology, electrophysiology and sequence homology:

- i) AMPA receptors, which are composed by the subunits GluR1-4
- ii) kainate receptors, composed by two of the subunits GluR5-7, KA1 and KA2
- iii) NMDA receptors, hetero-tetramers that contain both NR1 and NR2 subunits, and in some cases NR3. (W. Vandenberghe & D.S. Bredt, 2004)

AMPA receptors (AMPA receptors) mediate most excitatory (depolarizing) currents in conditions of basal neuronal activity. They have a major influence in the strength of the synaptic response.

The strength of the connection between a presynaptic and a postsynaptic neuron often exhibits a remarkable degree of plasticity. Synaptic transmission can be either enhanced or depressed, and these alterations can last from a transient few milliseconds to days, weeks or perhaps longer. Such changes in efficacy of synaptic transmission are likely to be important for a number of aspects of neural function.

Like other multimeric cell membrane proteins, GluRs are synthesized, folded and assembled in the endoplasmic reticulum. The reticulum endoplasmic is an organelle found in all eukaryotic cells and responsible of the production and storage of many macromolecules. They move then to the Golgi, a cell's organelle specialized in the processing and packaging of macromolecules, where the misfolded or misassembled GluRs are sorted (W. Vandenberghe, D.S Bredt, 2004). They have then to be transported to the synapses where they will form the receptors. All these movements are made in vesicles. GluR2-GluR3 oligomers are continuously delivered into synapses, such that the total number of AMPARs is preserved. GluR1-GluR2 and GluR4-containing receptors are added in a manner dependent upon NMDAR activation. This activation results in the opening of an ion channel which is nonselective to cations. Calcium flux through NMDARs is thought to play a critical role in synaptic plasticity.

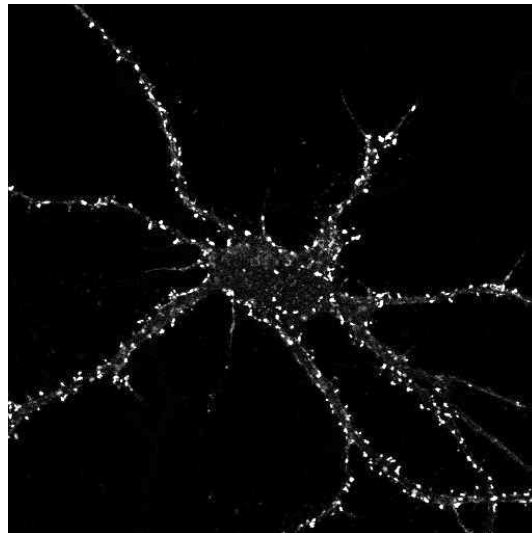


Fig. 5: Fluorescence confocal microscopy image of a neuron which AMPA receptors are labeled with Alexa 488. The image clearly shows the clustering behavior of the AMPA receptors, during their trafficking as well as during their fixation on the synapses. This image has been taken and gracefully lent by Michel Kropf, Laboratoire de Neurobiologie Cellulaire (LNC), EPFL, Switzerland

The interest in the plasticity of the synapses leads then to the observation of the movements of AMPARs. In order to localize them, the GluR1 unit can be labeled by an Alexa488 fluorescent molecule. The receptors are actually trafficking and fixed in the synapses in clusters. Figure 5 shows a confocal microscopy image of a neuronal cell marked with Alexa 488.

3. Experimental setup

The neuron samples are prepared by the researchers of the *Laboratoire de Neurobiologie Cellulaire* (LNC), EPFL, Switzerland. They extract neurons of 7 days old rats and let them grow in a special biological medium for two weeks, using the technique of transfection to label the AMPA receptors with Alexa 488. These molecules have the property of being excited resonantly by light with a wavelength very near 488 nm. At the end of the operation, the cells are fixed on a coverglass and the receptors on the surface of the neurons are fluorescently labeled.

Most of the time, the biologists use confocal microscopy to image the neurons, which makes it possible to excite locally the sample in deep. This technique gives fast and three dimensional results. The local excitation avoids a too fast photobleaching of the fluorophores in the regions next to what is under measure.

To overcome the limits of the confocal microscopy, namely the diffraction limit, an aperture SNOM in illumination mode is the appropriate configuration. This assembly is especially needed for fluorophores because far-field illumination would provoke the photobleaching of the Alexa, even before it is scanned. Contrary to the confocal microscopy, SNOM needs a long time of measurement, typically one hour for a $25 \times 25 \mu\text{m}^2$ area.

Our SNOM is a powerful tool because it allows us to obtain three different images of the sample during a single scan: topographical, fluorescence and transmission image. The experimental setup consists of a homemade SNOM scanning module mounted on a

conventional inverted microscope of type Olympus IX71 (D. Vobornik, 2005). The combination of a SNOM and a standard optical microscope is very useful to target the object to scan in the near-field. It's possible to place the starting point of the probe quite precisely, check the horizontal amplitude of the scan, control if the sample is not totally bleached or if it suffers the consequences of an uncontrolled contact with the tip. Actually, the projection of the laser beam on the sample which can be observed through the ocular is also a helpful indication during the manual approach of the tip to the sample.

In order to get high resolution optical images, we need a tip with a very small aperture. However, if the aperture is too small, our signal will be too weak and the noise will cover the signal. So we have to find the balance between these two. The SNOM optical probes were fabricated starting from singlemode silica fibers (with outside diameter 125 μm and core approximately 5.5 μm) using standard micropipette puller (D.T. Schaafsma & al., 1999). The tip geometry is highly important because it governs two crucial aspects of near-field imaging: lateral resolution and transmission efficiency. The mechanical characteristics determined by the shape of the probe are important as well, because they play a central role in the shear-force regulation of the SNOM probe.

The pulling process is a cycle of two-step processes, beginning with heat delivery from the source concurrent to a constant weak (gravity) pulling force; when a specified pulling velocity is achieved, then the pulling force is switched to a high (solenoid) pulling force, after which the heating is terminated. The two-steps process repeats itself until the material being pulled breaks or pulls apart (G.A. Valaskovic & al., 1995). The change of the heating and pulling parameters gives rise to very different probe shapes with different optical properties, discussed in this paper. The tips are then mounted in a modified vacuum evaporator where they are coated with gold. This coating is an optical guide avoiding light lost before the tip's aperture. This increases the optical resolution since the emitted spot is more concentrated. The tips which we use are provided by Antonio Cricenti, *Istituto di Struttura della Materia, CNR, Rome, Italy*. These probes have short tapers which should ensure a better coefficient of transmission.

The tip is attached to an oscillating dither-piezo-actuator. A bimorph-piezo fixed between them measures the amplitude of oscillation by giving an AC voltage signal. All this is placed on an x-y-z scanner. The x-y movements bring the probe from point to point while the z-piezo is involved in a feed-back loop and regulates the height of the tip in order to keep the sample-tip distance constant. (A. Cricenti & al., 1998)

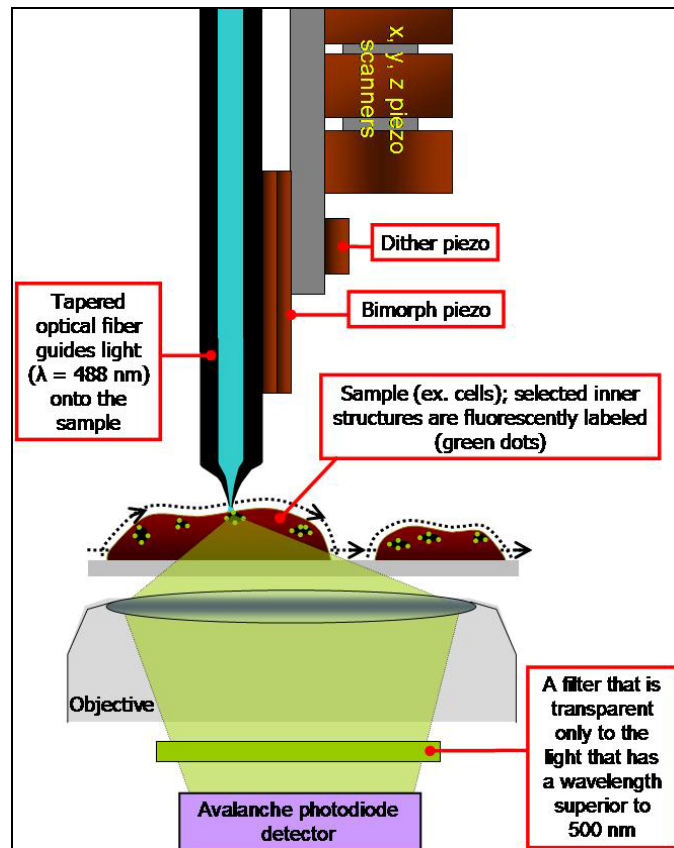


Fig. 6: Fluorescence SNOM Experimental Scheme (D.Vobornik, 2005)

The light source is an Argon ion laser from LG-laser technologies with a spectral distribution from 458 to 514 nm, where the emission peak at 488nm is the most powerful (80% of the total power output). This peak is the right wavelength to excite the Alexa488 molecules. Using a grating, the total beam is separated in its spectral components and the ray of the wanted wavelength is selected by a mirror and sent to a lens-based interface which injects the light into the optical fiber. Several adjustments are possible on the beam/fiber interface. The position of the objective in the vertical plane, its inclination and

the distance between the fiber entrance and the objective are adjustable in order to have the best intensity and focus of light in the fiber and consequently at the aperture.

Since there is a lot of noise in our signal due to residual light and vibrations, and since the signal that has to be detected is very weak, we use a chopper and a lock-in to select the desired signal and amplify it. The lock-in receives the signal from the photodetectors and “extracts” from the original signal the component which has the same frequency as the chopper. It amplifies this signal and transfers it to the Data Acquisition/Control Unit, which sends the signal to the computer.

To improve the quality of the measurements, particularly of the topography, all the equipment (in the dashed red rectangle of figure 7) is mechanically isolated on a pneumatic suspension table.

The high numerical aperture (1.4) oil immersion objective of the Standard Olympus microscope is used to collect the light coming from the sample which is then separated in two beams by a beamsplitter. One part of the light goes through a filter to an avalanche photodiode. The filter cuts the light having a wavelength smaller than 500nm. In that way, the avalanche photodiode doesn't detect the excitation light which passes simply through the sample or undergoes Rayleigh diffusion. It is selective to the light arising from inelastic scattering. In this way, most of the contribution is coming from the emission of the fluorophores, since the emission of stimulated Alexa is at 519nm. This detector is then the fluorescence signal recorder.

The second part of the light is sent to a photomultiplier which collects the entire light passing through the sample. This is the transmission signal. The beamsplitter can be readjusted by a groove. So, it is possible to change the proportion of light going to each detector. Since the emitted light from the fluorophores is quite weak, the groove should be adjusted so that at least 80% of the light goes to the avalanche photodiode.

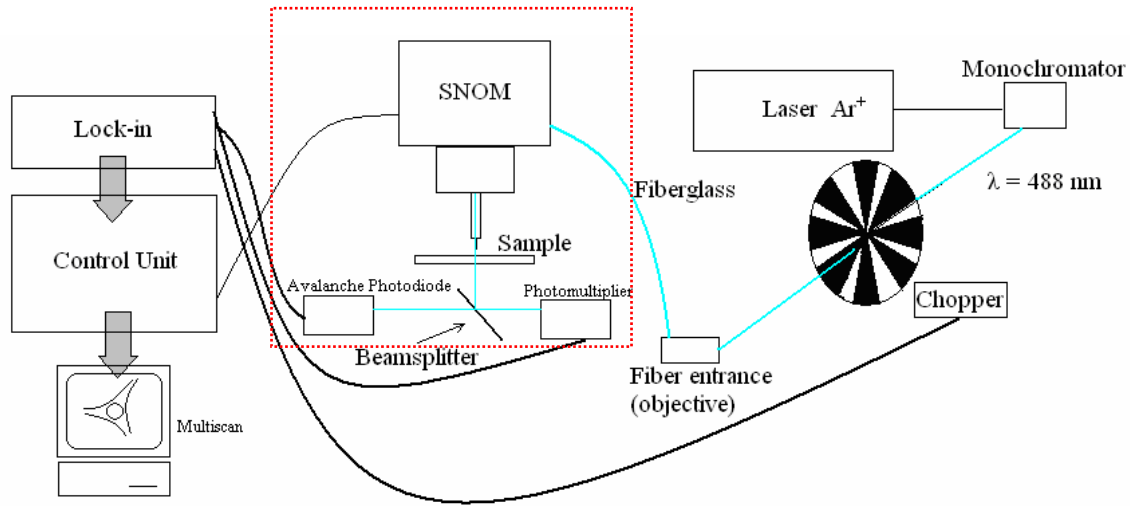


Fig. 7: Experimental Setup

With the used scanning software (Multiscan 95), we have directly on the computer screen the possibility to change all the relevant scanning parameters. Excluding some scaling parameters, which permit to relate the electrical tensions measured on the piezo-actuators with the real move of the tip, there are several parameters which can depend on the tip under use and which are simultaneously involved in the optical quality and in the quality of the scan.

At first, it is possible to adjust the size of the scanned area and the number of scanned lines, which corresponds to the number of points per line, since we are working with square areas. This parameter is of course very important for the optical resolution of the three images. However, a too high number of pixels will lead to a very long total time of scanning. We typically work on 25 μm square areas with 250x250 points.

It is also possible to change the integration time and the number of sample registered per point. The first one gives the time during which the signal coming from one optical detector is recorded and the second one is a statistical parameter which enables to average several measurements taken on the same point. A further parameter, called slew rate parameter, determines the speed of the horizontal movements of the tip when it turns back after each scanned line. These three values, together with the number of points and

the area surface, determine the horizontal movements of the tip. All these parameters influence also the quality of the optical signal, either directly or as a consequence of bad tip behavior.

Some other tip control parameters can be changed on the control unit. First of all one can change the frequency of the alternative voltage which excites the dither piezo carrying the tip. The control unit provides also an AC output which measures the voltage oscillations on a bimorph piezo fixed on the probe. This makes it possible to visualize the amplitude of oscillation on an oscilloscope. The goal is to work very near the resonance frequency of the piezo, which is slightly modified by the position of the tip taped on it and the weight of the glue. So, it has to be at least readjusted each time the tip is changed.

There are different theories about the best choice of the frequency to use. Recent works (D.A. Lapshin & al., 2004) showed that working with a slightly out of resonance probe leads to a more stable dynamics and the tip operates in a contact mode. Good results were shown on many samples including biological ones. So, we chose to work just under the resonance frequency, which is situated around 3.7 kHz. We noticed sometimes that bringing the probe to its resonance frequency give rise to a suddenly very noisy signal, while working slightly out of resonance leads to a clear sinusoidal signal.

After having fixed the frequency, the amplitude of the excitation can be changed. The control unit is also equipped with an AC/DC converter which gives as output the measured amplitude of the bimorph piezo. This DC value is called DCshear. It's also possible to change the gain of this AC/DC converter. Since our biological samples present very high structure (up to 4 μ m) and since the tip has to scan the surface at a distance of approximately 10nm, the only way is to use the SNOM in the constant force mode. A reference voltage can be introduced for that on the software panel which will be compared with the DCshear tension coming from the control unit and corresponding to the amplitude of the oscillation of the probe. When the tip goes near the sample, the shear forces are damping the oscillation. The software gives the reference voltage to the control unit which works as a feedback system: it changes the z-position of the tip by acting on

the vertical piezo-actuator so that the amplitude of oscillation corresponds to the reference voltage (C. Barchesi & al., 1997).

In our measurements, we worked typically with an AC amplitude of 10 mV, while the DCshear value was readjusted from one measure to the other. In fact, the values of the reference voltage and of the DCshear determine how far the probe will be from the sample's surface during the scan. This is a very important parameter for the optical signal, since evanescent waves decrease exponentially with the distance to the tip. To maximize the high resolution optical signal coming from the sample to the detectors in the far-field, it would be ideal to be as near as possible to the surface. This condition is limited by the technological possibilities and by the fact that a sufficient distance is necessary to ensure a good operation of the tip during the scan.

If we only use the topographic mode, the tip scans an area up to $40 \times 40 \mu\text{m}^2$ in the x-y plane and 8 μm in the z direction in a similar way as an Atomic Force Microscope (AFM). One can obtain a topographic image of the surface of the sample by keeping the tip-sample distance constant and by recording the z-motion of the tip.

A last parameter of the control unit which acts on the dynamics of the probe is the gain of the feedback loop. This value determines how fast the z-piezo reacts to a difference between the reference voltage and the DCshear. An optimal gain has to be found. A too high value leads to a very noisy topographical signal, because the tip reacts very fast and with great movements to small roughness on the sample surface. On the contrary, a too low value can cause a crash of the tip on the surface. This value of the gain depends strongly on the topography of the sample scanned. A smooth surface will be better measured with a small gain while a rough topography needs a higher gain. All this scanning control system and the exact meaning of the parameters are explained in details in the literature (C. Barchesi & al., 1997). Also the choice of a certain adjustment for some general parameters is discussed. For example, as described by this group, we decided to put the reference voltage value for the feedback system to about 70% of the DCshear signal measured when the tip is far from the sample.

As we learned from different measurements, it is very important to adjust correctly all these dynamical parameters of the tip before trying to improve the quality of the optical images by changing the lock-in adjustments.

The next step is to register the optical signals. Both for the fluorescence signal and for the transmission one, we use a lock-in. This system is coupled to the chopper which transforms the continuous beam coming from the laser in a train of impulses. The lock-in receives the entire optical signal coming from the photodetector and selects the component which has the same frequency as the chopper. In that way, the optical perturbations coming from other light sources than the laser are eliminated. For this it is important to choose a chopper frequency which is not a multiple of 50 Hz. In this particular case, the lock-in would be also registering the signal coming from the residual ambient light which works with a sinusoidal AC tension of 50 Hz. To minimize at best the optical pollution, we made all our measurements in the dark.

We have two types of lock-in available: an analogical and a digital one. The digital one has the advantage that it can set automatically the phase. This parameter is actually the time delay the lock-in is waiting after the start of each chopper pulse to register the signal. It has to be chosen so that the measured signal is positive (since we are measuring optical intensities) and maximized. It is possible to choose the time constant which determines the time window during which the signal is integrated to be then converted to an intensity value. This value is expressed in Volts and is then transmitted to the acquisition software. A too low value of the time constant will give rise to a very noisy signal while a too long time constant will lead to a signal which is averaged over a long time duration and harm in that way the optical resolution. Once again, we have to find the balance between these parameters.

Since the optical signal coming from the fluorescence detection chain is very weak, it is quite impossible to find manually the phase on the analogical lock-in. So, we decided to use the digital lock-in for the fluorescence measurement, at least to find the phase of the

signal which could be then introduced in the analogical lock-in. The transmission signal which is much more intense was measured by the analogical lock-in.

4. Experimental results and discussion

4.1. First results and transmission contrast:

In the first part of our experiments, we tried to optimize the parameters in order to have at first good topographical images. This is motivated by the fact that a bad tip behavior leads inevitably to more or less scrambled optical images, affected by scanning artifacts. As soon as the topography is of good quality, the scanning process is working well and the optical parameters can be adjusted on the lock-ins.

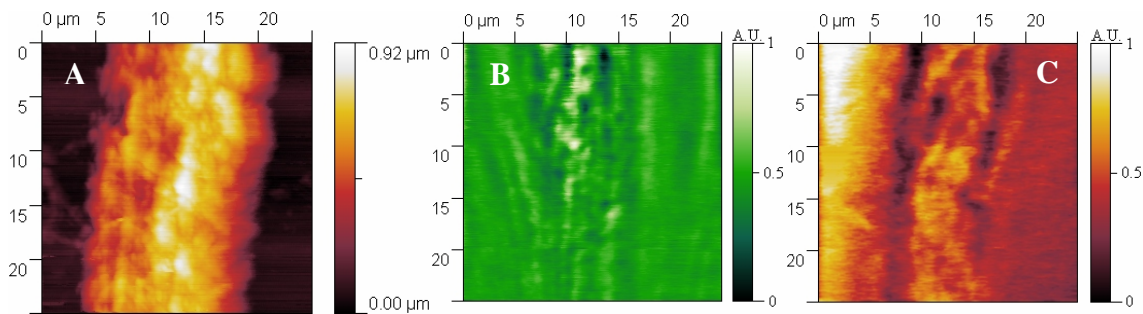


Fig. 8: A) 25 μ m square topography image of a hippocampal neuronal axon, with 250 pixels per line. B) Fluorescence recording. The intensity is in arbitrary unit. C) Transmission signal. The intensity is in arbitrary unit. The borders of the axon give rise to a strong contrast due to myelin absorption.

Figure 8A shows a 25x25 μm^2 picture of an axon. For all our measurements, the image resolution is 250x250 pixels. Micrograph shows that an axon of a hippocampal neuron has a typical height of $\sim 1 \mu\text{m}$. Further measurements show that dendrites are on the contrary significantly smaller and thinner, except the apical dendrite. This is a way for us to distinguish between these two types of neuronal channels. These observations are backed by the fact that axons have a typical myelin gain that dendrites don't have. By looking through the standard Olympus microscope, we can also notice that the axons have a very well defined direction and are quite straight whereas dendrites form rather complex networks.

The figure 8B presents the fluorescent measurement of this axon. The strongest intensity is measured on the axon. After applying a cubic fitting through the *Gwyddion* software, we can clearly see that clusters of fluorescence are appearing. This can be interpreted as the coagulation of receptors, similar to those shown in figure 5 taken with confocal microscopy. This confirms that we are measuring something relevant. However, individual points are not visible in the clusters. Optical fringes on the picture are visible, especially on the left side. This is possibly due to some interference of the ingoing light with itself. In fact, this picture was taken with all the spectrum of the laser. Since the filter cuts only the wavelength shorter than 500nm, it is possible that we are observing interferences between some components of the laser spectrum which are just going through the sample or are refracted by the sample without interacting with the fluorophores. The coherent light of the laser can be actually a limitation since the coherence area is not negligible on a near-field image and interferences are possible (C. Vannier & al., 2000). The use of all the spectrum of the laser can also lead to an image which is actually a combination of fluorescence and transmission measurement. This can be the cause of erroneous results.

In later measurements, we select the 488nm component of the laser. This avoids the formation of interference fringes since the ingoing light which does not interact with the fluorophores, thus going simply through the sample or being scattered in an elastic way, is simply blocked by the filter. We are then looking theoretically only to the light coming from the fluorophores, with about 519 nm wavelength.

The figure 8C is the image of the transmitted light through this sample. The only treatment applied on the image is a step line correction made with *Gwyddion*, since the transmission signal presents originally a step due to sensitivity adjustment on the lock-in during the scan. In fact, the sensitivity should be adjusted so that the range of intensity measured on the sample covers at best the 10 Volts range of the output signal of the lock-in. This is quite difficult to know *a priori* since the beginning of the measurement shows only the signal of the first lines and doesn't give global information about the optical

signal on the entire sample. This is why the measurements have often to be repeated twice. In that case, the input signal of the lock-in became stronger and stronger during the measurement until the input was near the overload. To avoid the overload for the rest of the images, which would lead to loss of information, we changed the sensitivity range during the scanning process.

Figure 8C shows that the sides of the axon absorb sensibly more light than the central part in this spectral range (green). This can be interpreted in the following way: inside the axon, there is the cytoplasm which is mostly made up of water and mineral salts. These materials don't absorb much in this spectral range. On the other hand, the wall is principally composed of lipids and proteins. The axons are in addition hedged in a thick lipid layer called myelin. The myelin is made up of a lot of different constituents. Several studies of rats' neurons (A. di Biase & al., 1990, E.R. Kandel & al., 1991, W. T. Norton & S.E. Poduslo, 1973) indicate that the most important components are lipids (~73 %) (mostly cholesterols and phospholipids (~50%)). Lipids are much more opaque to visible light than aqueous solutions. Of course, the membrane goes all around the axon but since the tip is always nearly vertical to the sample, the thickness of myelin crossed by the light is not the same on the middle of the axon than in the borders (figure 9). This change of thickness due to the geometry is the source of the border contrast of the axon.

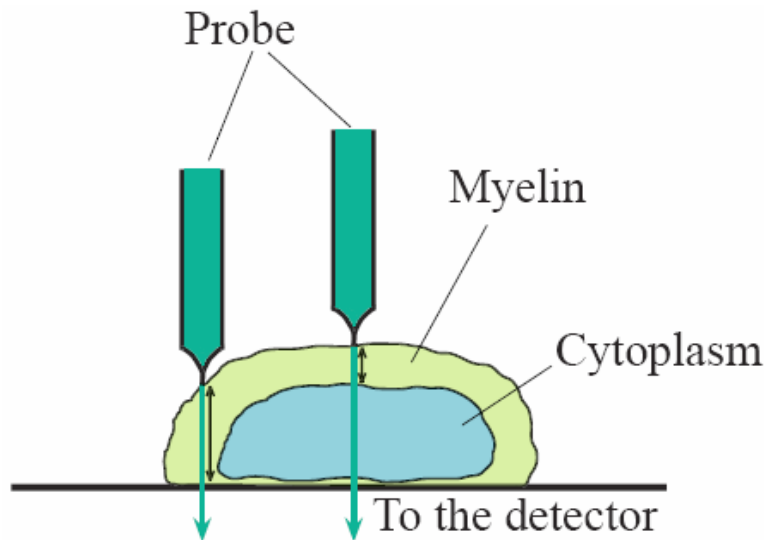


Fig. 9: Schematic cross-section view of the transmission border contrast of the axon due to the geometry of the observation.

4.2. Topography images and gradient analysis:

The images obtained after several changes of the settings of the scanning process are of good quality. This means that the noise is low in both x and y directions. The horizontal steps due to misalignment of successive scanned lines are sparse or small and the “accidents” due to stronger contact between the tip and the sample do not occur. We obtain then very smooth images of the cells and it is easy to obtain information about the localization of the structures which are then observed on the optical images. The geometry of the setup allows to put the tip in the desired position by watching the light spot of the tip on the sample through the optical wide-field Olympus microscope. The topography measurement is then a confirmation of the good positioning.

We are observing quite high structures compared to what is generally observed with SNOM. Since we are dealing with samples which are sometimes $4\ \mu\text{m}$ high, the simple look at the topography images doesn't give much information about the small details, since they are drowned in the main high structure. This is due to the fact that the color scale is calibrated to cover the entire height of the sample and small variations of the height (i.e. details) don't give any contrast on the images. For this reason, everything looks quite smooth and like “unfocused”.

To obtain the hidden information of the topography, one possibility is to analyze the local variation of the height of the topography. This can be simply done by looking at the magnitude of the gradient vector in each point of the topography. We decided to implement this directly on the *interactive data language* software (IDL). We took the gradient in each direction by looking at the average height of the two next points of the given pixel and the average height of the two previous points. The averaging of the two next points avoids too strong oscillations of the gradient from one point to the other due to residual noise. The result of this simple operation gives an image with enhanced details. The contrast between the structures is sharper and reveals new information about the analyzed sample. Figure 11 shows results taken on neuron bodies. This gradient

analysis is especially interesting in very high structures like neuron bodies. On dendrites, the simple topography shows already sufficiently details.

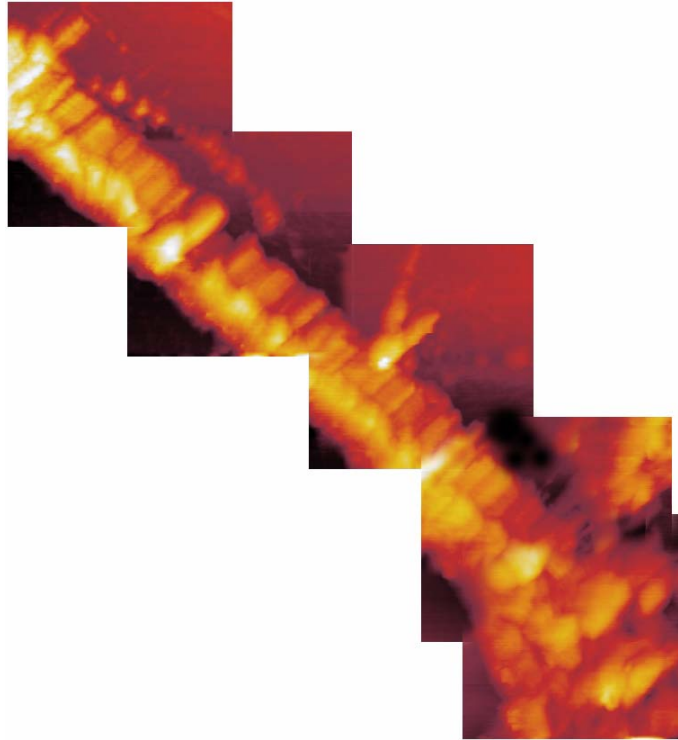


Fig. 10: Juxtaposition of 25 μm square topography images of neighboring areas giving an overview of an axon. The change of position from one area to the next one is done manually. The adjustment of two adjacent images is made by fitting similar details observed on both images.

Since we are measuring the change of topography, the irregularities of the images are enhanced in the gradient analysis. These images are in that way a real proof of the good quality of the topography images. Erroneous points give rise to crosses in the gradient, which are for example visible on figure 11 B3.

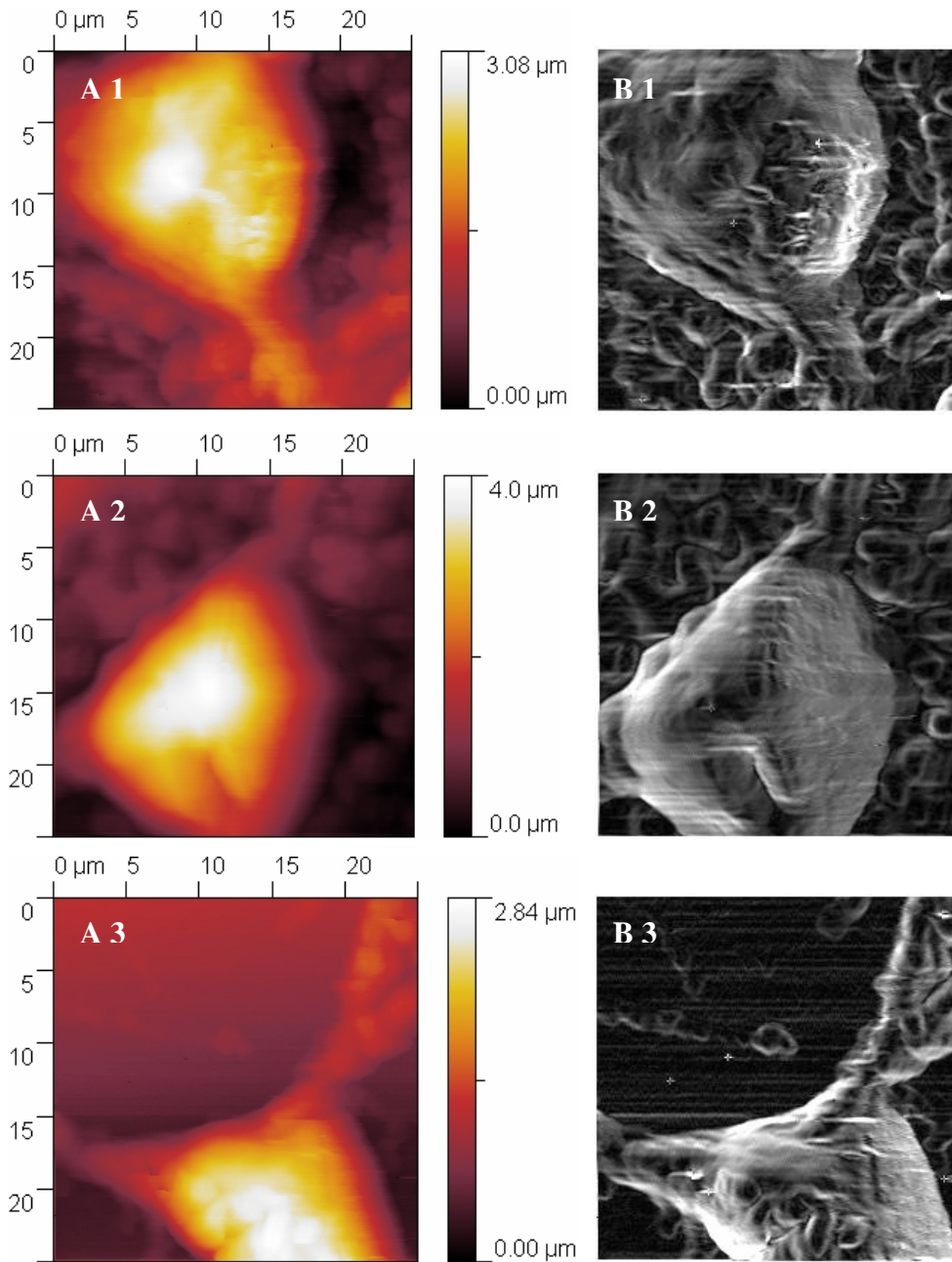


Fig. 11: A) 25 μm square topography images of neurons' bodies. The details are lost due to the color scale fitted to the big height of the overall structure. B) Images of the two dimensional gradient of the topography. These images give information about the slope of the sample. In that way, the small details are also visible.

However, these phenomenons are really isolated and negligible. We can also have a good idea of the surface of the surrounding area. Sometimes the cell is surrounded by a complex network of dendrites of other cells like it is the case in figure 11 B1 or the cell is

quite isolated on the coverglass as shown in figure 11 B3. This is a good indication to interpret the signal coming from the optical measurements.

4.3. Resolution analysis:

The determination of the optical resolution is of great interest, since it is the main feature of the SNOM. However, its determination is not obvious. Already in classical microscopy, the optical resolution is subject to discussion. In fact, it is necessary to determine a resolution criterion. The most used is the Rayleigh criterion. In SNOM, the solution is more complicated. It is nearly impossible to define a transfer function of the microscope like it is possible in classical microscopy. This transfer function has the property of defining the power of resolution of the microscope independently from the sample. Since the tip is a very complicated diffractive object, the only theoretical way is to work with approximations.

In first approximation, considering the tip as a passive object collecting the waves above the sample, the amplitude of the evanescent wave associated to the horizontal spatial frequency $2\pi/\Delta x$ decreases like:

$$\exp\left(-\frac{2\pi}{\Delta x} z\right)$$

where z is the distance between the tip and the sample and Δx is the size of a diffracting object on the sample.

So, it is possible to define a typical resolution in function of the distance between the tip and the sample z :

$$\Delta x \approx 2\pi z \quad (\text{D. Courjon \& C. Bainier, 2001})$$

Since we are working with our SNOM with the shear-force regulation in constant tip-sample distance mode, the z should be constant and the resolution is expected to be the same on the entire image. However, the shear forces depend on the nature of the surface under the tip. Some topographical artifacts are then possible if the tip goes over different types of surface. An area can also appear brighter than another even if in reality it is just the opposite. An example of inverted contrast on samples of aluminium structures on

silicon dioxide is given in the literature (R.L. Williamson & al., 1998). This is possible if the shear forces on this area have a shorter range. To maintain a given amplitude of oscillation, the tip will be driven lower. Since the intensity of the evanescent waves decrease exponentially with the z distance to the tip, a small tip-sample distance change can cause a big difference in the evanescent light reaching the sample surface and consequently in the intensity of light coming from the sample to the far-field detectors.

The resolution depends among others on the illumination conditions, the polarization, the tip shape or size and the distance between tip and sample. All this parameters are often unknown or approximately known. For that reason, most evaluations are based on the visual inspection of the images obtained, like it is the case for our work.

The resolution calculation has to be done carefully. The resolution calculated by the image analysis is not directly a characterization of the setup but the result of its interaction with the sample. The observations are then spectral analysis of the image including the specificities of the scanning probe microscopy. We already mentioned the problem of the tip-sample distance. The scanning movements bring also inhomogeneity in the images. In fact, drifts of the scanning piezos may produce steps in the topography. This means that the sample-tip distance changes and so the resolution. This is a problem for global two dimensional resolution analyses. The only reliable resolution analyses have to be done along scanning lines. Due to uncontrolled parameters, the resolution can be different from one part of the image to the other. It is then necessary to study the resolution in the most local possible way. (D. Courjon & C. Bainier, 2001)

4.3.1. Two dimensional Fourier analysis:

At first we would like to show the information coming from the two dimensional Fourier transform and the problems encountered by this analysis. This analysis presents the advantage that it is easy to carry out and most image processing softwares are able to perform it. We have done this analysis by using the *Gwyddion* toolkit. The analysis is made with a Hamming window and Bspline interpolation. The colors represent the module of the Fourier coefficients. Figure 12 shows the 2D Fourier analysis of a raw topographical measurement made on a piece of dendrite.

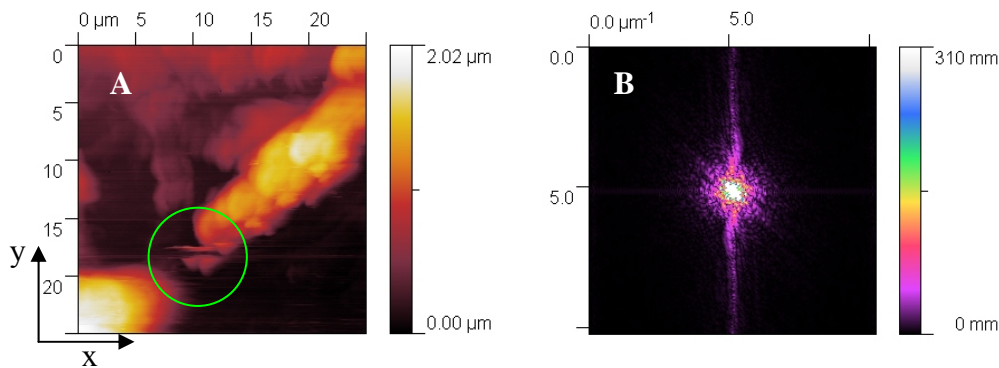


Fig. 12 : A) 25 μm square topography image of a dendrite. There are 250 scanned lines and 250 points per line. B) 2D Fourier transform of image A. The spectrum shows clearly a vertical line arising from scanning artifacts. Each line is not exactly aligned to its neighbors and this gives a strong high frequency signal in the direction perpendicular to the scanned lines.

The vertical line appearing on the analysis is a typical syndrome of a scanning artifact. All our images are constructed by putting the horizontal scanned lines one above the other. Steps or drifts in the scanning piezo-actuators lead to steps or oscillations in the vertical direction. This leads in the Fourier analysis to wave vectors in the vertical direction, like it is visible on figure 12B. This line is appearing more or less on each image, depending on the quality of the y motion of the probe. Clearly, it is very unlikely that this line would arise from structures on the sample, since we have scanned a lot of different areas and since this line was always vertical. We can see by eye that the image is of good quality excluding the structure hedged by the green circle which is a scanning

artifact, possibly arising from tip rubbing, which doesn't appear on a successive scan of the same area.

The Fourier analysis is then much more sensitive to these discontinuities than the human eye. The image resulting from the analysis shows the wave vectors contained in the data. Since the module of the wave vector is inversely proportional to the wavelength of the Fourier component, we see that this artifact interferes with the high frequency components of the signal. These high frequency components are actually the object of interest to determine the resolution of the image. Moreover, since this analysis takes into account the entire signal in a global way, it is not possible to make the distinction between the real resolution and the artifactual one arising from the noise. The Fourier analysis gives a very fine resolute analysis in the frequency domain but gives no information about the location on the sample of the structures presenting a given Fourier spectral component. A way to obtain this location information is to work with windowed Fourier transform. We present further another local spectrum analysis, namely the wavelet analysis, which presents some advantages in comparison with the windowed Fourier transform.

However, the 2D Fourier transform is a way to have a better view of the y scanning artifacts, since it gives prominence to the vertical high frequency components. Figure 13 shows an example on a topographical measurement which presents two steps probably due to tip rubbing (see fig. 13A). In fact, the tip came into strong contact with the sample. This contact was sufficiently strong to destroy the cell under measure and to push parts of it away. This fact could be easily seen at the end of the scanning process by looking through the Olympus wide-field optical microscope.

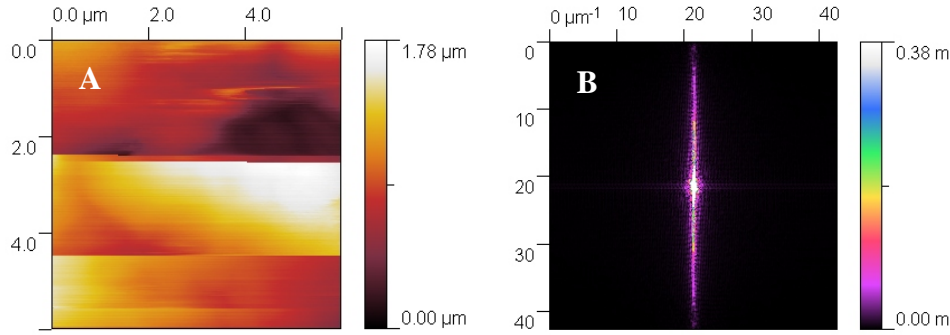


Fig. 13: A) 5 μm square transmission image of part of a neuron body, with 250 pixels per line. The color scale represents the intensity of light passing through the sample in arbitrary unit. B) 2D Fourier analysis of A realized with the software *Gwyddion*

The Fourier coefficients of the vertical wavevectors are much more present in this image, due to the steps in the vertical direction of the shear-force micrograph. This example is of course quite extreme and the visual inspection would certainly be sufficient to detect these artifacts. Nevertheless, it shows the ability of the 2D Fourier transform to make the experimentalist aware of scanning artifacts and it also shows the impossibility to get reliable information about the resolution (i.e. about the high frequency signal) with 2D standard methods.

Figure 14 shows the same analysis made on a transmission optical image. The y scanning artifact is not very pronounced, ensuring that the transmission signal has a real significance, like we could expect from visual inspection. However, this shows that the optical signals are also affected by the y scanning artifact. The optical signal depends exponentially on the tip-sample distance and is in that way interrelated with the topographical irregularities. This means that even with a well regulated tip-sample distance, there is still a problem of alignment between two scanned lines and that it has also to be taken into account in the optical images. This underlines the fact that one cannot give correct resolution information in the vertical direction by 2D transforms. The different nature of the horizontal and vertical lines doesn't make possible to define a resolution in two dimensions like it is possible in classical images.

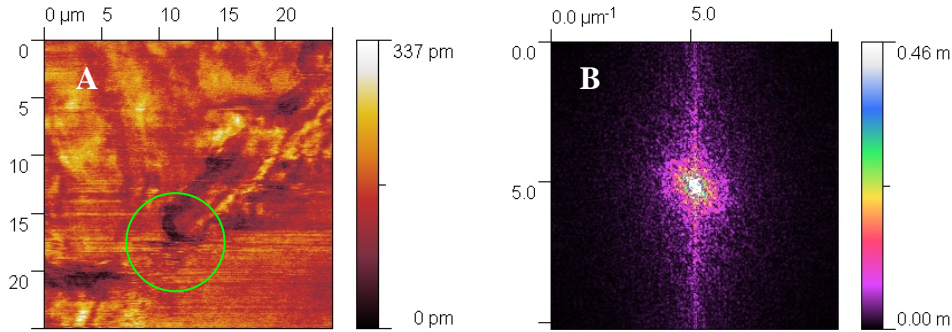


Fig. 14: A) 25 μm square transmission image of a dendrite, with 250 pixels per line. The color scale represents the intensity of light passing through the sample in arbitrary unit. B) 2D Fourier analysis of A realized with the software Gwyddion

The transmission image of figure 14A was taken simultaneously with the topography of figure 12A. The area in the green circle shows that the horizontal structure originating from the tip rubbing visible on the topography corresponds to a black line in the transmission. This is another example of the influence of the movements of the tip on the optical measurements. This black line is a diminution of the transmitted light, possibly due to the bending of the tip or to its temporary removal from the sample. Other observations of this artifactually high resolution in the direction perpendicular to the scanned lines have been made by other groups (T.Gharbi & D. Barchiesi, 2000)

4.3.2. Discrete wavelet analysis:

Space localization of spectral components can be obtained by multiresolution wavelet analysis, as this method provides the space-frequency representation of the signal. Among many space-frequency representations, the discrete wavelet transform (DWT) has become increasingly popular due to its ability to solve a diverse set of problems, including data compression, biomedical signal analysis, feature extraction, noise suppression, with modest computational expense.

The DWT analyzes the signal at different frequency bands with different resolutions through the decomposition of the signal (multiresolution analysis). The DWT utilizes two sets of functions: scaling functions and wavelet functions, each associated with lowpass and highpass filters, respectively. Decomposition of the signal into different frequency

bands is accomplished by successive highpass and lowpass filtering of the space domain signal.

For the 1D wavelet analysis, the original signal is a line of scan obtained with the SNOM. This set of pixels forms an array of real numbers called $x[n]$ where n is the coordinate of each pixel. The result of the lowpass filter with impulse response g is a discrete convolution of x and g :

$$y[n] = (x * g)[n] = \sum_{k=-\infty}^{\infty} x[k]g[n - k]$$

The signal is also decomposed simultaneously using a highpass filter h . The output gives the detail coefficients (from the highpass filter) and approximation coefficients (from the lowpass filter). In terms of angular frequency the sample frequency is 2π . According to Nyquist-Shannon rule (S. Mallat, 1998), the highest frequency in the sample is then π . After the application of the filters, the highpass signal contains the frequency components between $\pi/2$ and π and the low pass signal those between 0 and $\pi/2$. According to the Nyquist-Shannon rule, since the lowpass signal has a maximum frequency of $\pi/2$, half of the sample points can be eliminated by downsampling.

The resolution is bound to the quantity of information in the signal. It is affected by the filtering which eliminates half of the frequencies and corresponds therefore to the loss of half of information. The downsampling divides by two the number of samples of the filtered data, redundant in any case. This filtering and downsampling is mathematically expressed by:

$$y_{high}[n] = (x * g)[n] = \sum_{k=-\infty}^{\infty} x[k]g[2n - k]$$

$$y_{low}[n] = (x * h)[n] = \sum_{k=-\infty}^{\infty} x[k]h[2n - k]$$

This decomposition divides by two the spatial resolution in both channels (lowpass and highpass) due to the downsampling but this operation doubles the frequency resolution since the frequency band is divided by two. The frequency uncertainty is divided by two. The idea is then to repeat this operation on the coefficients obtained by the lowpass filter.

Repeating this operation, one can construct a multiresolution tree, since each level of decomposition analyzes the signal at different frequency ranges and different resolutions.

These notions are developed and explained in detail by Stéphane G. Mallat (S.G. Mallat, 1989). The filters must satisfy several conditions to avoid redundancy and to keep the maximum of information about the starting signal. This principle was at first developed for the compression of data. In fact, an inverse operation makes it possible to reconstruct the initial data from the different channels. If the filters are not ideal half-band filters, the reconstruction cannot be performed. Under certain conditions, one can find filters which enable the perfect reconstruction. The most famous are those developed by the Belgian physicist Ingrid Daubechies, the Daubechies wavelets (I. Daubechies, 1988).

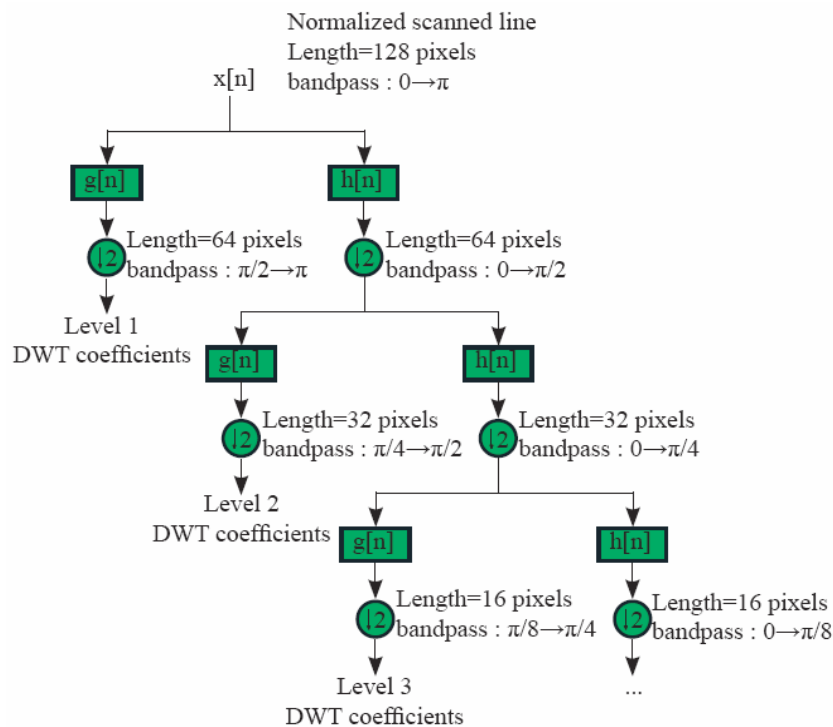


Fig. 15: Diagram of the multiresolution discrete wavelet analysis

Due to the decomposition process, the input signal must be a multiple of 2^n where n is the number of levels of the multiresolution decomposition. For our analysis, the multiresolution tree can be imaged by the scheme presented on figure 15.

A big advantage of the discrete wavelet analysis in comparison with the windowed Fourier analysis is the quality of the spectral filter. An example is shown in the literature (T. Gharbi, D. Barchiesi, 2000), comparing the hamming filter of the Fourier transform with two types of Daubechies wavelets (figure 16).

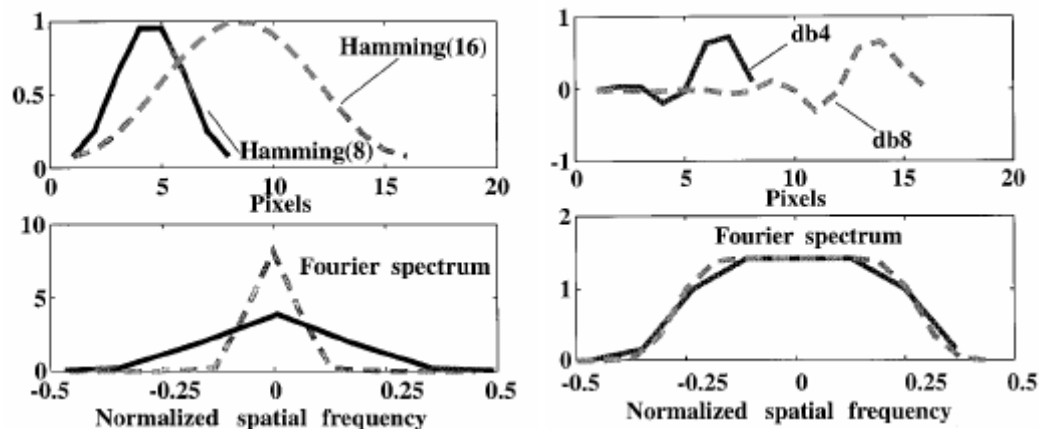


Fig. 16: Comparison of the spectral filters of the windowed Fourier analysis with those of the wavelet analysis (T. Gharbi, D. Barchiesi, 2000). The abscissas is the normalized frequency (i.e. (period of the signal in pixels)⁻¹). A) Hamming windows used in windowed Fourier transform. B) Daubechies wavelets (dbN has a length of 2N) and the associated modulus of the discrete Fourier transform spectrum.

In order to decompose a signal in its frequency components, the best filter would be ideally a square filter, with a constant gain under the cut-off frequency and a null gain above it (S. Mallat, 1998). In practice, there are several types of wavelets and the choice is not trivial. We chose to work with Daubechies wavelets which present spectral filters near the ideal square filter. The Daubechies wavelets are named with the number of vanishing moments M they have (dbM). This is defined as the higher number M so that for $m < M$ we have:

$$\int_{-\infty}^{\infty} x^m \psi(x) dx = 0$$

The example of figure 16 shows that a higher vanishing moment gives rise to a steeper filter. On the other hand, a wavelet with a higher vanishing moment has a larger support

and is more sensitive to discontinuities (D. Lemire and G. Pau, 2006). To summarize, a higher vanishing moment gives a better filter but a worse spatial resolution. Since the choice of a wavelet is still a matter of discussion and that it depends strongly on the analyzed sample, we tried several wavelets and selected the most significant one by visual comparison with the original sample. From this point, to simplify the discussion about the resolution (given in pixels), we will speak from spatial frequencies in pixels by suggesting actually the corresponding spatial wavelengths.

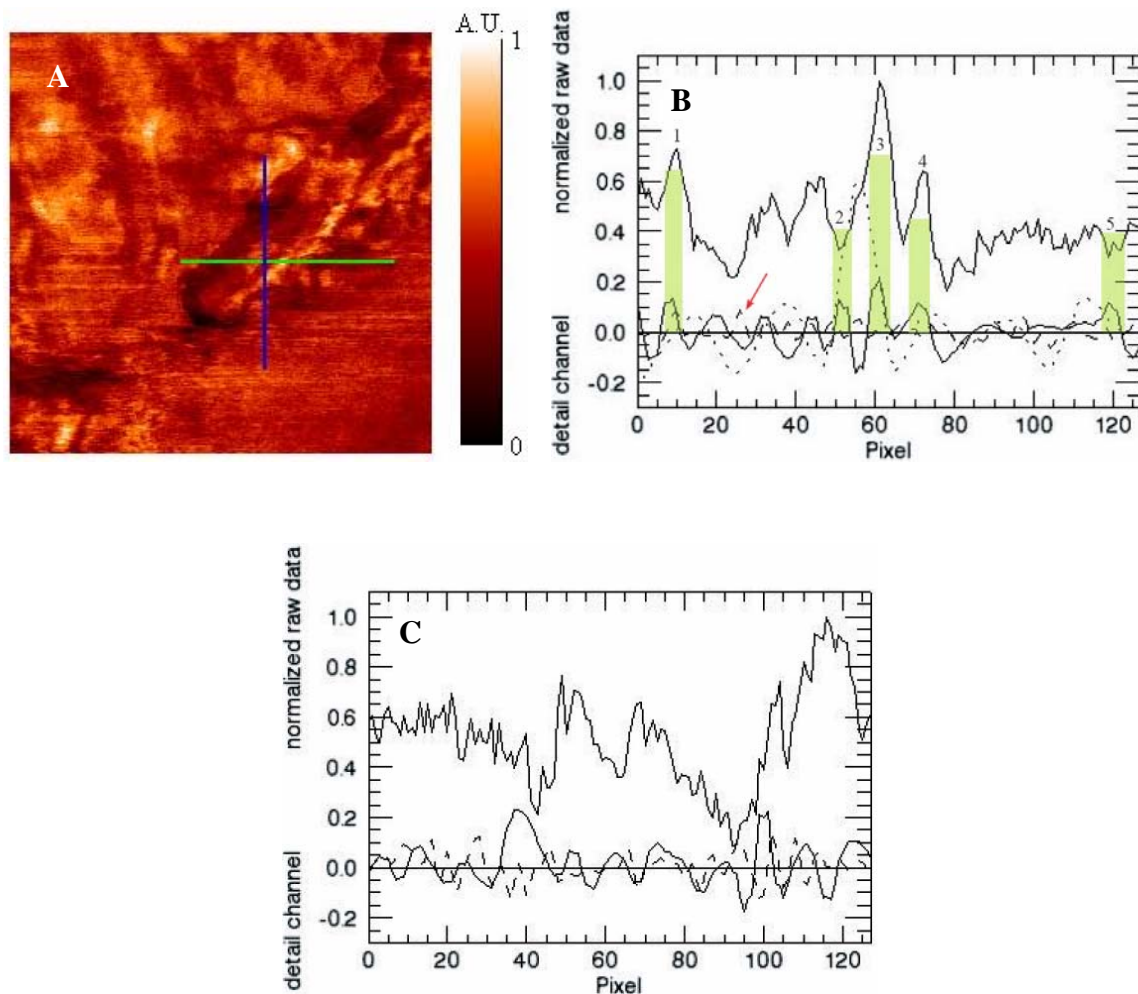


Fig. 17: A) $25\ \mu\text{m}$ square transmission image of a dendrite, with 250 pixels per line. B) Horizontal cross-section of A (green line) and detail channels of the multiresolution analysis. The dashed line is the level 1 signal, the solid line the level 2 and the dotted line the level 3. Since these levels have respectively 64, 32 and 16 samples points, they are scaled to 128 pixels and fitted with a cubic spline interpolation. C) Level 1 (2 pixels to 4 pixels frequency components) and level 2 (4 pixels to 8 pixels frequency components) of the multiresolution analysis of the vertical blue profile.

Figure 17 shows two cross-sections of a transmission image taken on a dendrite. The green horizontal line on A corresponds to the profile in panel B and the vertical blue line to the profile in panel C. Figure 17B presents the detail channel of level 1 (dashed line), level 2 (solid line) and level 3 (dotted line) of the multiresolution analysis made with the wavelet Daubechies 5. In details, level 1 shows where the signal has a frequency component between 2 and 4 pixels, level 2 between 4 and 8 pixels and level 3 between 8 and 16 pixels. Figure 17B shows that the optical transmission signal presents several structures with about 4 pixels resolution. The main structures are underlined. This resolution is particularly clear between the areas 2 and 4. However, the 2 pixels component of the structure 1 is also important. The red arrow presents another area with a predominant 2 pixels component. This corresponds to a stiff slope on the raw data. This means that there are parts of the profile which have a resolution between 2 and 4 pixels whereas others have at best a resolution of 4 pixels, like the areas 2,3 and 4.

This corresponds actually to the rough optical resolution determination, observing the full width at half maximum of the peaks 3 and 4 which gives respectively 7 and 5 pixels. The change of the resolution is the main motivation of this wavelet analysis. The possible localization of the high resolution area through this analysis makes it possible to differentiate the noise from the real signal resolution. This is necessary since the SNOM images are inhomogeneous. A similar analysis made by T. Gharbi and D. Barchiesi (T. Gharbi & D. Barchiesi, 2000) shows that the spatial frequencies can vary drastically from a zone of the image to another.

Figure 17C presents the detail channels of the level 1 and 2 of the multiresolution analysis of the blue vertical profile. This example shows that the 2 pixels component is much more important in this direction due to scanning artifacts like discussed in the 2D Fourier analysis. However, the absence of high peaks in the 2 pixel channel certifies that the image is not suffering of an intensity step due to the scanning, like discussed in the literature (T. Gharbi & D. Barchiesi, 2000). So, the vertical structure of the transmission image is meaningful. Nevertheless, an objective resolution analysis can only be made in the horizontal direction.

This analysis shows that we are reaching a resolution varying between 3 and 6 pixels, which corresponds to 300nm to 600nm. I should be recalled that this is not the absolute resolution possibility of the setup. In fact, to have a meaningful detail channel, the image must present a structure with a given spatial frequency. The multiresolution algorithm analyses the image and not the setup. Actually, since a sampled signal cannot contain a signal with a wavelength smaller than 2 pixels (Nyquist-Shannon sampling criterion), a multiresolution analysis will never give a resolution smaller than 200 nm in our case (1 pixel = 100nm). To analyse the resolution deeper, it is necessary to perform the analysis on an image with a higher pixel density.

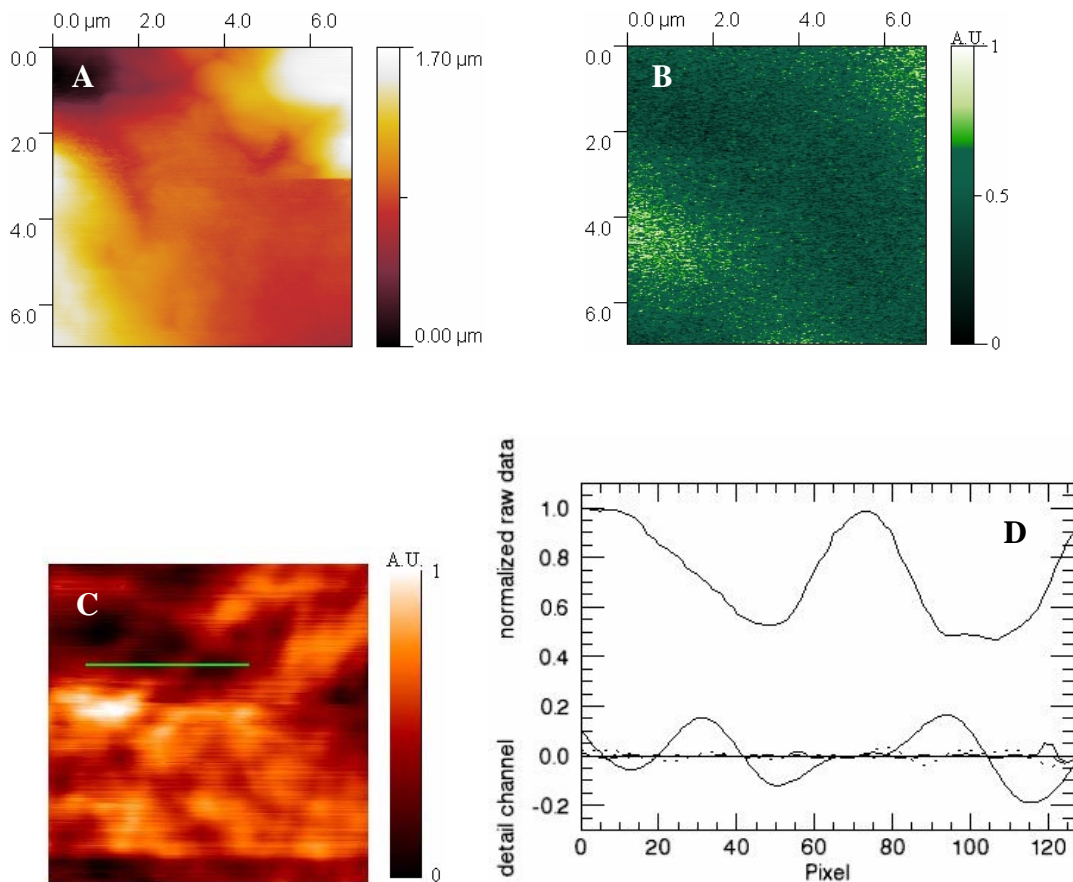


Fig. 18: A) 6,5 μm square topography of a part of a hippocampal neuron body, with 250 pixels per line. B) Fluorescence recording on this area C) Recording of the transmitted light. The green line shows the profile taken as sample for the multiresolution analysis D) Horizontal cross-section of C (green line) and detail channels of the multiresolution analysis. The first channel with significant amplitude is the detail channel of level4 which corresponds to the spatial frequencies between 16 and 32 pixels.

Figure 18C presents a 6,5 μm square transmission recording made on a cell body of the hippocampal neurons culture. This image displays prominently the possibilities of the transmission measurements. It appears clearly that the transmission gives new information about the sample and is not simply correlated to the topography. The transmitted light gives actually not only information about the thickness of the sample but also about the optical density of what is inside the cell. Since, we are still working with 250 pixels per line, the Nyquist-Shannon frequency limit is then at about 52nm which is 2 pixels in this image. It means that the multiresolution analysis is able to find out the frequency components of the transmission signal down to 52nm.

Figure 18D shows the multiresolution analysis of a horizontal profile of the transmission image, drawn in green on figure 18C. The sample is 128 pixels long and the wavelet used is Daubechies 5 (vanishing moment =5). The detail channels of the four first levels of decomposition are shown. The first channel with significant coefficients is the detail channel of the level 4. This channel contains the signal with spatial wavelength from 16 to 32 pixels. This means that the best resolution reached on this measurement can be estimated at 16 pixels, which corresponds roughly to 420nm. This is quite in agreement with the measurements made previously on larger areas (i.e. with lower pixel density). The Nyquist-Shannon criterion is no more a limit in the resolution determination on this sample. Other studies on other parts of this sample give the same type of result.

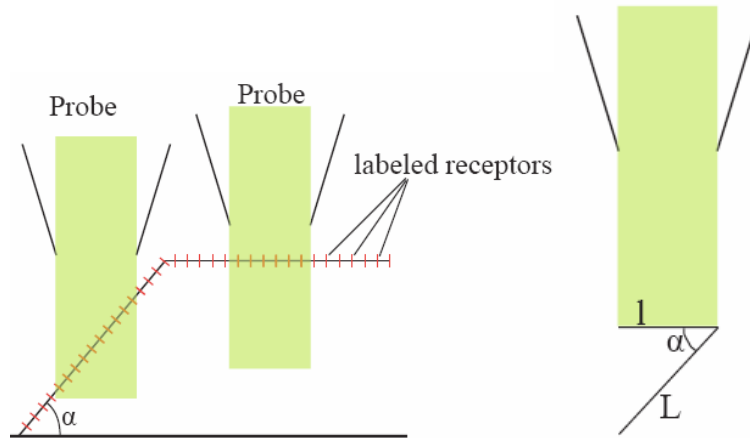
It has to be mentioned again that the “resolution” found by wavelet analysis is in fact the spatial frequency analysis of one image. The found value depends on the structure present on the sample. A real resolution determination for the transmission measurement is possible by multiresolution analysis if an image is taken on a reference absorption grating with well-known dimensions.

4.4. Fluorescence emission:

In all our SNOM measurements, the most difficult signal to obtain is the fluorescence. This is due to the very low light intensity emitted by the fluorophores. Even if more than 80% of the outgoing light beam is sent to the fluorescence detection chain, it is difficult to obtain a high signal to noise ratio. The low transmission efficiency of the tip and the limited interaction cross-section of the fluorophores are the limits imposed to the fluorescence SNOM. The quality can be improved by increasing the power of the laser. This enhancement has to be kept in some limits since a too high beam power would lead to an overheating of the tip and possibly to its destruction. However, after many adjustments, we were able to obtain images with significant information on the fluorophores.

4.4.1. Fluorescence correction:

On several images, a correlation between the cell borders visible on the topography measurements and the fluorescence is observable. This behavior is similar to the border contrast in the transmission. In fact, the labeled receptors are supposed to be on the surface of the cell, namely in the membrane. Since the tip is always vertical, it is not perpendicular on every point to the sample surface. This is particularly true for samples with high structures like those we have observed. For this reason, a similar labeled receptors density on the membrane can give rise to a change in the measured intensity, due to the geometry of the observation. This is illustrated on figure 19. A correction could then be made to be sure that we are not just observing a border effect. Assuming in a rough approximation that the tip is illuminating the sample with a vertical beam with a constant square cross-section, the number of excited receptors is bigger if the sample surface is inclined. This simple approximation is a first step in a decorelation of the fluorescence signal from the topography. The correction in that case can be made by multiplying the measured intensity by the cosinus of the angle formed with the horizontal in both x and y directions. The procedure implemented on *IDL* gives the result shown on figure 20 C.



The light intensity emitted by the labeled receptors is proportional to the number of excited receptors. This number is equal to the density of receptors multiplied by the illuminated length.

$$I \propto N_{\text{receptors}}$$

$$N_{\text{receptors}} \propto \rho_{\text{receptors}} \times L$$

Let l be the cross-section of the beam and L the illuminated length. We have :

$$l = \cos(\alpha)L$$

So, on horizontal surfaces, we have : $I \propto \rho_{\text{receptors}} \times l$

And on inclined surfaces :

$$I \propto \frac{\rho_{\text{receptors}} \times l}{\cos(\alpha)}$$

To obtain the same information about the density of receptors on all surfaces, one has then to multiply the measured intensity by $\cos(\alpha)$. With the approximation of a beam with constant square cross-section, we can do this in both x and y directions by multiplying the measured intensity by $\cos(\alpha)$ and $\cos(\beta)$ where α and β are respectively the angles in the x direction and in the y direction measured on the topography.

Fig. 19: Description of the correction process applied to the fluorescence measurement to subtract the contribution due to the geometry of the measurement.

The borders of the cell appear very clear on the corrected image. The dark color means that the corrected intensity is low. This result shows that the sample has been actually overcorrected, since the borders appear much darker than the surrounding area which should actually give no or very low fluorescence signal. Our approximation seems to be too coarse. This is due to several reasons. At first, the beam is not a simple beam with a

constant square cross-section but is similar to a cone (G.A. Valaskovic & al., 1995). The intensity of the evanescent waves is decreasing exponentially with the distance to the tip. This means that the receptors which are further from the probe are less excited and emit less light. Moreover, nothing insures that all the receptors in the beam receive the same intensity. The homogeneity of the beam depends on the aperture of the tip. It could also happen that some of the receptors are shadowed by some structures and receive less excitation light since the inclined surface can be rough. Our approximation can be consistent only for small angles. For bigger angles, the problem becomes much more complicated and the knowledge of the beam structure of the probe and of the exact distance between the probe and the sample is necessary.

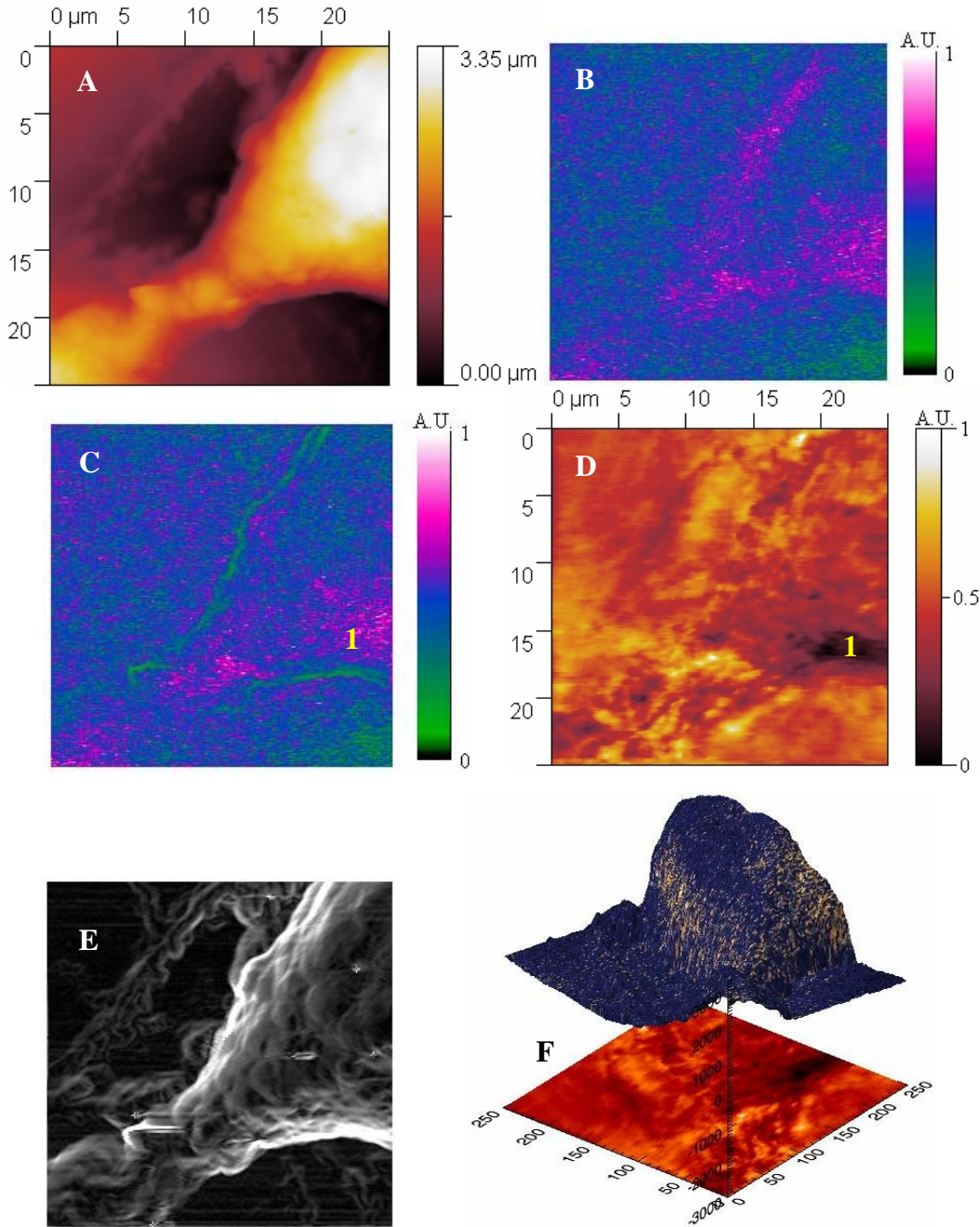


Fig. 20: A) 25 μm square topography of a part of a neuron body and a dendrite, with 250 pixels per line. B) Image of the fluorescence. The scale goes from green to pink in increasing light intensity. C) Corrected fluorescence image using the process described in figure 19. The correction on the sharp edges is too strong. D) Transmission image of the same area. Black corresponds to low intensity and thus to opaque structures. E) Image of the gradient magnitude of the topography image. This operation has the property of displaying the borders of the structures independently of their relative height. In that way, small structures next to bigger ones are still recognizable. F) 3D view of the topography with the fluorescence applied on it. A non negligible part of the higher fluorescence emission is located on the border of the cell body (height in nanometer and horizontal dimensions in pixels: 1 pixel=100nm). The image on the bottom corresponds to the transmission signal.

4.4.2. Global results and discussion:

The strong fluorescence correction of the figure 20C shows that even with an overestimated correction, there is still fluorescence near the border, revealing that the measured quantity is not only noise enhanced by border effects. Figure 20C shows also that a higher intensity is measured in the area labeled with the number 1. This corresponds to a dark region in the transmission. This is of great interest. The fluorescence light goes also through the sample like the total beam measured by the transmission chain. In that way, it undergoes nearly the same absorption than the transmission signal. The fact that a dark region in the transmission corresponds to a bright one in the fluorescence confirms that the fluorescence recordings really come from the selecting binding of the fluorophores and are not the result of an absorption contrast between different areas.

Moreover, we can assume that the densest part of the internal structure of the cell body is the nucleus. This one is also surrounded by an organelle called endoplasmic reticulum. The most probable position of the nucleus is then the darkest region of the transmission inside the cell. It means then that we observe higher surface concentration of receptors near the nucleus. We know from the theory of the receptors' trafficking (E.R. Kandel & al., 1991) that the receptors are produced in this area. It seems then that for a 7 days old rat, the highest concentration of receptors is located near the nucleus. This observation is in concordance with some biological models presented in the literature (H. Adesnik & al., 2005).

The measurements made on another cell body in figure 21 confirm this analysis since the image presents the same correspondence between the area with the brightest fluorescence emission and the darkest zone in the transmission assumed to be the nucleus.

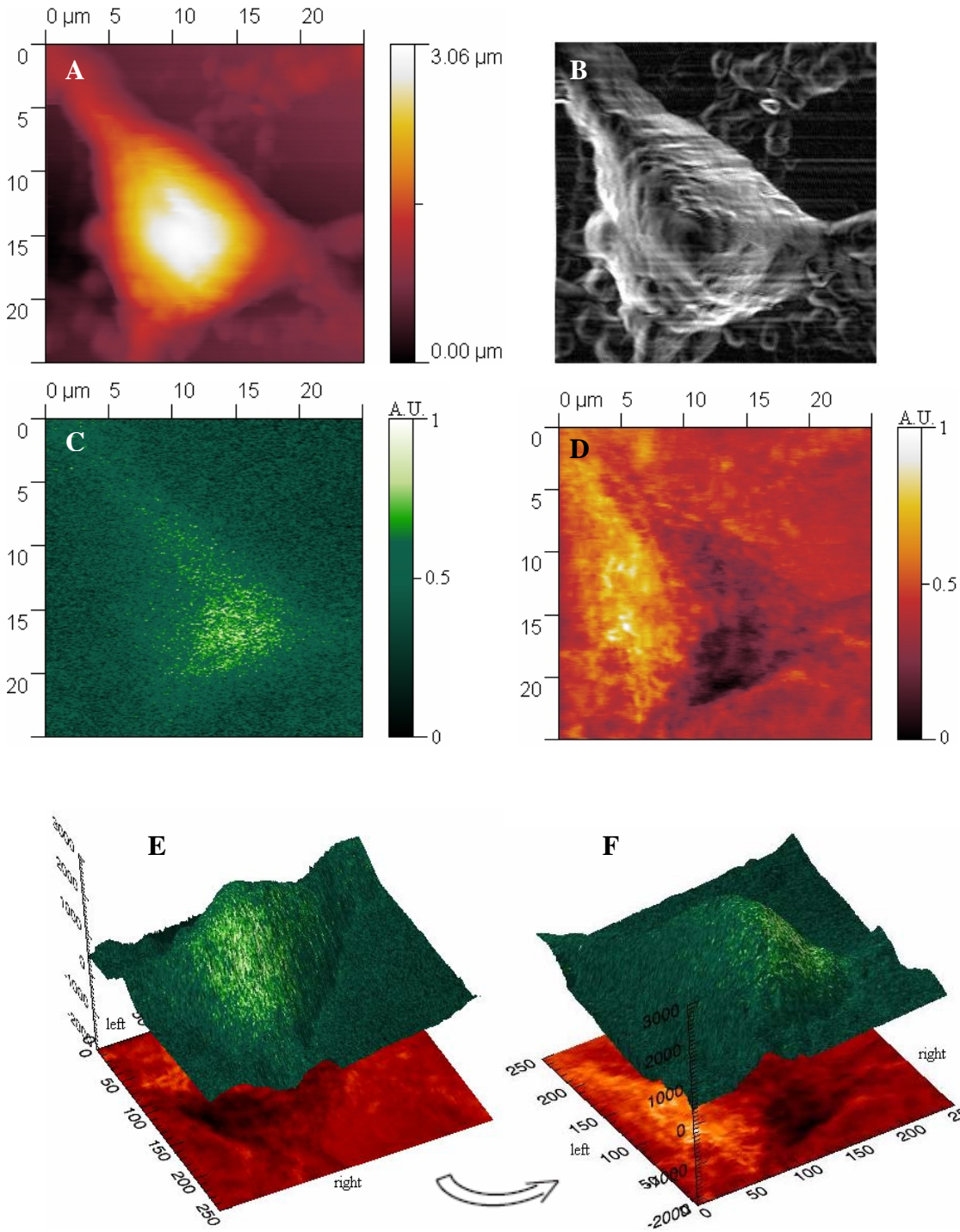


Fig. 21: A) 25 μm square topography of a neuron body, with 250 pixels per line. B) Gradient analysis of the image A. C) Fluorescence recording. The intensity is in arbitrary unit. D) Transmission signal. The intensity is in arbitrary unit. The darker area is supposed to be the nucleus (densest organelle of the neuron). E) and F) Two 3D images of the topography with the fluorescence applied on it. The point of view is changed from E to F to show that the fluorescence is mostly located on one side of the cell, namely on the same side as the nucleus. The image on the bottom is the transmission signal.

An important point for our SNOM measurements is also that the highest structure in the topography is not inevitably the brightest area in the fluorescence. This means that the fluorescence signal is not an artifact due to uncontrolled tip-sample distance regulation. Actually, such problems could appear since we are working with high structures and that the amplitude of movement could approach the limits of the vertical piezo regulator. Figure 20 confirms thus that the distance regulation is working well. This fact is also clear on figure 21.

Figure 21 presents a complete set of measurements, containing the topography, the fluorescence and the transmission signals. The structure present in the scanned area is a neuron body. This image is particularly interesting because the fluorescence measurement underlines that its intensity is not strictly correlated to the slope of the topography. In that way, it confirms that we are really measuring a quantity directly linked to the concentration of labeled receptors. The border effect is not predominant. This becomes even clearer on the three dimensional images of the topography of figure 21 E and F with the fluorescence applied on it. These pictures show the structures from two different points of view. The “right” front of the neuron presents a strong fluorescence emission whereas the “left” side is much darker, nearly comparable to the ambient noise.

The low transmission in the area 1 of figure 20C could also be explained by the absorption of the fluorophores located in this region. This would contradict our interpretation of this dark spot as the position of the nucleus. However, other measurements (figure 22) show that the superposition of the fluorescence maximum with the lowest transmission spot is not always the case. Thus, our first explanation of the absorption spot seems coherent. A quantitative analysis of the influence of the absorption of the fluorophores on the transmission signal should be done with reference samples.

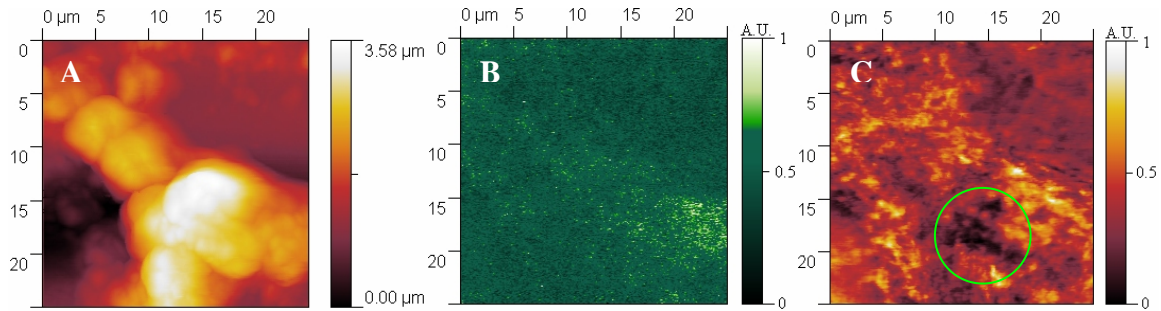


Fig. 22: A) 25 μm square topography image of a neuron body. B) Fluorescence emission. C) Transmission signal. The darkest area of the transmission doesn't correspond to the highest emission area of the fluorescence. This gives support that this dark spot arises from the internal structure of the cell and is not due to fluorophore absorption.

These examples show that the transmission image gives some more information about the sample. It doesn't only show a specific shape corresponding to the topography but it informs also about the internal constituent of the cell. The recording of the transmission is therefore a piece of information which shouldn't be neglected in further measurements. Moreover, since the part of the splitted beam going to the transmission detection chain is lower than 20% of the total beam, there is still enough light intensity going to the fluorescence detector. Actually, by trying to improve the signal to noise ratio in the fluorescence, we divided by two (reaching 10% of the total light intensity) or sometimes more the intensity going to the transmission without noticing a relevant decrease of quality of the transmission signal. In this way, we can pretend that the transmission measurement is not interfering much on the quality of the fluorescence recording.

The transmission signal on cell body gives regularly a dark region which is assumed to correspond to the densest part of the cell inside, namely the nucleus. We can see that we are in that way independent of relatively inexact assumptions concerning the position of the nucleus. In fact, if the transmission is not observed, the first idea is to assume that the nucleus resides in the part of the cell with the highest structure (M. Koopman & al., 2004). We see in the example of figure 20 and figure 21 that it is not always in agreement with the more precise information given by the transmission. The transmission gives us key parameters to understand the fluorescence.

5. Conclusions and perspectives

The good quality of the topography measured by our SNOM gives more information than just the right positioning of the sample. Its smoothness, clearly visible in the quality of the gradient images, is a proof of a good scanning process. This ensures that the optical images carries really information about the optical properties of the sample and are not scanning artifacts due to the tip's rubbing or bending. Our measurements show also that the feed-back system and the piezo actuators are completely able to perform the measurements on high structures like the cell bodies of the neurons.

The transmission gives us more information about the sample since it is sensitive to the inner constituents of the sample. The multiresolution analysis shows a resolution down to about 400nm which is good since we are looking at inner structures. The simple visual inspection of these images shows the usefulness of this measure and the comparison with electronic microscopy images could certainly lead to a better identification of the structures appearing on this images. The ease of performing transmission measurements and their small influence on fluorescence imaging makes this kind of study a very useful tool. A better determination of the ability of our SNOM in transmission could be done by analyzing reference samples such as absorption grids.

The fluorescence signal is the hardest to register, since its intensity is very low, and is thus much noisier. It reaches the limits of the potential of our setup. The result is not clear enough to detect clusters of fluorescence but the analysis of the distribution of the intensity on the neurons' body tends to confirm other biological observations. One way to improve the quality of the fluorescence measurement would be to increase the intensity of the incident light. This could be done by using a better device to select the 488 nm spectral component from the laser beam and by improving the efficiency of the coupling interface between the laser beam and the entrance of the optical fiber.

The assembling of the scanning actuators on the sample instead of on the tip could also lead to a more stable dynamics which would improve the quality of all the measurements channels.

Although the topography and transmission images of our SNOM setup gives significant results, we see that better fluorescence results are certainly possible and would also lead to a high resolution detection of the fluorescence. A quantitative analysis of the light intensity at each level of the SNOM setup would be a way to determine where the main loss of intensity occurs. A quantitative analysis with reference samples could also give more information about the importance of the resonant absorption of the fluorophores on the transmission signal.

6. Acknowledgments

First of all, I would like to thank Prof. Davor Pavuna who gave me the motivation to reach his laboratory and who was open to all types of discussions about physics and the physicist's life during my master project semester but also during the physics practical works of my fourth year of study. His highly positive view of the physics is contagious. Speaking with him gives the impression that nothing is impossible.

My best thanks go to Johanna Generosi who took all the necessary time to teach me the subtleties of the scanning near-field optical microscopy. She always rendered me assistance while giving me gradually more and more autonomy. In this way, I also felt myself progressively involved in this research topic. Her unconditional support went beyond what can be expected from a master project assistant.

I would like also to thank Vincent Gajdošík for all his help in the computer processing I undertook on the IDL software environment. He also found the time to reuse and adapt parts of the Multiscan software codes to give me direct access to the source data without the loss of information due to changes of formats.

7. Bibliography

(in the alphabetical order)

- E. Abbe, *Archiv. Mikroskop. Anat.* **9** (1873) 413
- H. Adesnik, R. A. Nicoll and P. M. England, *Neuron* **48** (2005) 977
- E. A. Ash and G. Nicholls, *Nature (London)* **237** (1972) 510
- C. Barchesi, A. Cricenti, R. Generosi, C. Giammichele, M. Luce and M. Rinaldi, *Review of Scientific Instruments* **68** (1997) 3799
- D. Barchiesi and T. Gharbi, *Applied Optics* **38** (1999) 6587
- D. Barchiesi and T. Gharbi, *European Physical Journal Applied Physics* **5** (1999) 297
- M.V.L. Bennett, *Nature Neuroscience* **3** (2000) 7
- A. Di Biase, S. Salvati and G.S. Crescenzi, *Neurochemical Research* **15** (1990) 519
- G. Binnig, H. Rohrer, C. Gerber and E. Weibel, *Applied Physics Letters* **40** (1982) 178
- G. Binnig, H. Rohrer, C. Gerber and E. Weibel, *Physical Review Letters* **49** (1982) 57
- G. Binnig, C. F. Quate and C. Gerber, *Physical Review Letters* **56** no 9 (1986) 930
- A. Callerari, *Molecular Physics course notes 2005*, LSU, EPFL, Switzerland
- D. Courjon and C. Bainier, *Le Champ Proche Optique: Théorie et Applications*, Editions Springer Paris, Paris, 2001
- A. Cricenti and R. Generosi, *Review of Scientific Instruments* **66** (1995) 2843
- A. Cricenti, R. Generosi, C. Barchesi, M. Luce and M. Rinaldi, *Review of Scientific Instruments* **69** (1998) 3240
- A. Cricenti, *Applied Surface Science* **162-163** (2000) 275
- A. Cricenti, *Journal of Alloys and Compounds* **328** (2001) 2
- A. Cricenti, G. Longo, M. Luce, R. Generosi, P. Perfetti, D. Vobornik, G. Margaritondo, P. Thielen, J.S. Sanghera, I.D. Aggarwal, J.K. Miller, N.H. Tolks, D.W. Piston, F. Cattaruzza, A. Flamini, T. Prosperi and A. Mezzi, *Surface Science* **544** (2003) 51

- A. Cricenti, V. Marocchi, R. Generosi, M. Luce, P. Perfetti, D. Vobornik, G. Margaritondo, D. Talley, P. Thielen, J. S. Sanghera, I. D. Aggarwal, J. K. Miller, N. H. Tolk and D. W., Piston, *Journal of Alloys and Compounds* **362** (2004a) 21
- A. Cricenti, G. Longo, A. Ustione, V. Mussi, R. Generosi, M. Luce, M. Rinaldi, P. Perfetti, D. Vobornik, G. Margaritondo, J. S. Sanghera, P. Thielen, I. D. Aggarwal, B. Ivanov, J. K. Miller, R. Haglund, N. H. Tolk, A. Congiu-Castellano, M. A. Rizzo, D. W. Piston, F. Somma, G. Baldacchini, F. Bonfigli, T. Marolo, F. Flora, R. M. Montereali, A. Faenov and T. Pikuz, *Applied Surface Science* **234** (2004b) 374
- A. Cricenti, Microscopy, *Scanning Near-Field Optical Microscopy*, 2005 Elsevier Ltd. (in press)
- I. Daubechies, *Commun. in Pure and Applied Math.* **41** (1988) 909
- R.C. Dunn, *Chemical Reviews* **99** (1999) 2891
- encyclopedia.thefreedictionary.com/Pyramidal+cells
- S. Fukura, T. Nakagawa and H. Kagi, *Diamond & Related Materials* **14** (2005) 1950
- M. Futamata and A. Bruckbauer, *Chemical Physics Letters* **341** (2001) 425
- T. Gharbi and D. Barchiesi, *Optics Communications* **177** (2000) 85
- Y. Goda and G. W. Davis, *Neuron* **40** (2003) 243
- B. Hecht, H. Bielefeldt, Y. Inouye, D.W. Pohl and L. Novotny, *Journal of Applied Physics* **81** (1997) 2492
- B. Hecht, B. Sick, U.P. Wild, V. Deckert, R. Zenobi, O.J.F. Martin and D.W. Pohl, *Journal of Chemical Physics* **112** (2000) 7761
- S. Hoppe, G. Ctistis, J.J. Paggel and P. Fumagalli, *Ultramicroscopy* **102** (2005) 221
- N.F. van Hulst, J.A. Veerman, M.F. Garcia-Parajo, and L. Kuipers, *Journal of Chemical Physics* **112** (2000) 7799
- A. Ianoul, M. Street, D. Grant, J. Pezacki, R. S. Taylor and L. J. Johnston, *Biophysical Journal* **87** (2004) 3525
- E.R. Kandel, J.H. Schwartz and T.M. Jessell, *Principles of Neural Science*, Third Edition, Appleton & Lange, Norwalk, 1991
- J.M. Kim, H. Hiroshi Muramatsu, H.Y. Lee and T. Kawai, *FEBS Letters* **555** (2003) 611

- J.M. Kim, T. Ohtani and H. Muramatsu, *Surface Science* **549** (2004) 273
- M. Koopman, A. Cambi, B.I. de Bakker, B. Joosten, C.G. Figdor, N.F. van Hulst and M.F. Garcia-Parajo, *FEBS letters* **573** (2004) 6
- F. de Lange, A. Cambi, R. Huijbens, B. de Bakker, W. Rensen, M. Garcia-Parajo, N. van Hulst and C.G. Figdor, *Journal of Cell Science* **114** (2001) 4153
- D. A. Lapshin, V. S. Letokhov, G. T. Shubeita, S. K. Sekatskii and G. Dietler, *Applied Physics Letters* **81** (2002) 1503
- D.A. Lapshin, V.S. Letokhov, G.T. Shubeita, S.K. Sekatskii and G. Dietler, *Ultramicroscopy* **99** (2004) 227
- Haw-Long Lee, Win-Jin Chang, Wen-Lih Chen and Yu-Ching Yang, *Ultramicroscopy* (2007) doi:10.1016/j.ultramic.2007.01.001 (in press)
- D. Lemire and G. Pau, <http://www.ondelette.com/forum/FAQ/French/faqondelette.pdf>, 2006
- S.G. Mallat, *IEEE Transactions on Pattern Analysis and Machine Intelligence* **11** (1989) 674
- S. Mallat, *A Wavelet Tour of Signal Processing*, Academic Press, San Diego, 1998
- W.E. Moerner, T. Plakhotnik, T. Irgartinger, D. W. Pohl, and B. Hecht, *Physical Review Letters* **73** (1994) 2764
- W. T. Norton and S. E. Poduslo, *Journal of Neurochemistry* **21** (1973) 759
- N. Panchuk–Voloshina, R. Haugland, J. Bishop-Stewart, M. Bhalgat, P.J. Millar, F. Mao, W.Y. Leung and R.P. Haugland, *Journal of Histochemistry & Cytochemistry* **47** (1999) 1179
- D.W. Pohl, W. Denk and M. Lanz, *Applied Physics Letters* **44** (1984) 651
- D.T. Schaafsma, R. Mossadegh, J.S. Sanghera, I.D. Aggarwal, J.M. Gilligan, N.H. Tolk, M. Luce, R. Generosi, P. Perfetti, A. Cricenti and G. Margaritondo, *Ultramicroscopy* **77** (1999) 77
- P. Steiner, *Membrane trafficking in neurons regulated by new syntaxin 13-interacting proteins*, PhD thesis no3091, EPFL, 2004
- R.M. Stöckle, V. Deckert, C. Fokas, D. Zeisel and R. Zenobi, *Vibrational Spectroscopy* **22** (2000) 39

- E. H. Syngé, *Philosophical Magazine* **6** (1928) 356
- G. Turrell and J. Corset, *Raman Microscopy: Developments and Applications*, Academic, Cambridge, 1996
- G. A. Valaskovic, M. Holton and G. H. Morrison, *Applied Optics* **34** (1995) 1215
- W. Vandenberghe and D. S. Bredt, *Current Opinion in Cell Biology* **16** (2004) 134
- C. Vannier, C. Bainier and D. Courjon, *Optics Communications* **175** (2000) 83
- D. Vobornik, G. Margaritondo, J.S. Sanghera, P. Thielen, I.D. Aggarwal, B. Ivanov, J.K. Miller, R. Haglund, N.H. Tolk, A. Congiu-Castellano, M.A. Rizzo, D.W. Piston, F. Somma, G. Baldacchini, F. Bonfigli, T. Marolo, F. Flora, R.M. Montereali, A. Faenov, T. Pikuz, G. Longo, V. Mussi, R. Generosi, M. Luce, P. Perfetti and A. Cricenti, *Infrared Physics & Technology* **45** (2004) 409
- D. Vobornik, *Scanning Near-Field Infrared Microscopy and spectromicroscopy applied to nanosystems and cells*, PhD thesis no3296, EPFL, 2005
- S. Webster, D. A. Smith and D. N. Batchelder, *Vibrational Spectroscopy* **18** (1998) 51
- en.wikipedia.org/wiki/Synapse
- R.L. Williamson, L.J. Brereton, M. Antognozzi and M.J. Miles, *Ultramicroscopy* **71** (1998) 165
- softwares :
- interactive data language* software IDL, <http://www.itvis.com/idl/>
- Gwyddion analysis software*, <http://gwyddion.net/>
- Multiscan scanning software*, C. Barchesi, A. Cricenti, R. Generosi, C. Giammichele, M. Luce and M. Rinaldi, *Review of Scientific Instruments* **68** (1997) 3799